JOURNAL OF GEOPHYSICAL RESEARCH, VOL. 105, NO. E4, PAGES 9623–9642, APRIL 25, 2000

# Detection of crystalline hematite mineralization on Mars by the Thermal Emission Spectrometer: Evidence for near-surface water

P. R. Christensen,[1] J. L. Bandfield,[1] R. N. Clark,[2] K. S. Edgett,[3] V. E. Hamilton,[1] T. Hoefen,[2] H. H. Kieffer,[4] R. O. Kuzmin,[5] M. D. Lane,[6] M. C. Malin,[3] R. V. Morris,[6] J. C. Pearl,[7] R. Pearson,[2] T. L. Roush,[8] S. W. Ruff,[1] and M. D. Smith[7]

**Abstract.** The Thermal Emission Spectrometer (TES) instrument on the Mars Global Surveyor (MGS) mission has discovered a remarkable accumulation of crystalline hematite ($\alpha$-$Fe_2O_3$) that covers an area with very sharp boundaries approximately 350 by 350–750 km in size centered near 2°S latitude between 0° and 5°W longitude (Sinus Meridiani). Crystalline hematite is uniquely identified by the presence of fundamental vibrational absorption features centered near 300, 450, and >525 $cm^{-1}$ and by the absence of silicate fundamentals in the 1000 $cm^{-1}$ region. Spectral features resulting from atmospheric $CO_2$, dust, and water ice were removed using a radiative transfer model. The spectral properties unique to Sinus Meridiani were emphasized by removing the average spectrum of the surrounding region. The depth and shape of the hematite fundamental bands show that the hematite is crystalline and relatively coarse grained (>5–10 $\mu$m). Diameters up to and greater than hundreds of micrometers are permitted within the instrumental noise and natural variability of hematite spectra. Hematite particles <5–10 $\mu$m in diameter (as either unpacked or hard-packed powders) fail to match the TES spectra. The spectrally derived areal abundance of hematite varies with particle size from ~10% (>30 $\mu$m diameter) to 40–60% (10 $\mu$m diameter). The hematite in Sinus Meridiani is thus distinct from the fine-grained (diameter <5–10 $\mu$m), red, crystalline hematite considered, on the basis of visible, near-IR data, to be a minor spectral component in Martian bright regions like Olympus-Amazonis. Sinus Meridiani hematite is closely associated with a smooth, layered, friable surface that is interpreted to be sedimentary in origin. This material may be the uppermost surface in the region, indicating that it might be a late stage sedimentary unit or a layered portion of the heavily cratered plains units. We consider five possible mechanisms for the formation of coarse-grained, crystalline hematite. These processes fall into two classes depending on whether they require a significant amount of near-surface water: the first is chemical precipitation that includes origin by (1) precipitation from standing, oxygenated, Fe-rich water (oxide iron formations), (2) precipitation from Fe-rich hydrothermal fluids, (3) low-temperature dissolution and precipitation through mobile ground water leaching, and (4) formation of surface coatings, and the second is thermal oxidation of magnetite-rich lavas. Weathering and alteration processes, which produce nanophase and red hematite, are not consistent with the coarse, crystalline hematite observed in Sinus Meridiani. We prefer chemical precipitation models and favor precipitation from Fe-rich water on the basis of the probable association with sedimentary materials, large geographic size, distance from a regional heat source, and lack of evidence for extensive groundwater processes elsewhere on Mars. The TES results thus provide mineralogic evidence for probable large-scale water interactions. The Sinus Meridiani region may be an ideal candidate for future landed missions searching for biotic and prebiotic environments, and the physical characteristics of this site satisfy all of the engineering requirements for the missions currently planned.

## 1. Introduction

One of the primary objectives of the Thermal Emission Spectrometer (TES) instrument on the Mars Global Surveyor (MGS) spacecraft is to determine and map the mineralogic composition of the Martian surface. Of particular interest is the search for minerals formed through interaction with water, either by low-temperature precipitation or weathering or by hydrothermal mineralization. In this paper we describe the initial discovery, physical properties, spatial distribution, and origin of a concentration of crystalline hematite on the surface in the Sinus Meridiani region of Mars that we suggest most likely formed by a process (or processes) involving significant amounts of near-surface water.

The TES instrument measures the emitted infrared energy from ~6 $\mu$m (1606 $cm^{-1}$) to ~50 $\mu$m (201 $cm^{-1}$) with 5 and 10 $cm^{-1}$ spectral sampling [*Christensen et al.*, 1992]. The measured spectrum is the result of the emission, absorption, and transmission of energy by the surface materials and by $CO_2$, water ice, dust, and water vapor in the atmosphere. Each measured spectrum contains information on the temperature profile of the atmosphere, the abundance and temperature of

[1]Department of Geology, Arizona State University, Tempe.
[2]U.S. Geological Survey, Denver, Colorado.
[3]Malin Space Science Systems, San Diego, California.
[4]U.S. Geological Survey, Flagstaff, Arizona.
[5]Vernadsky Institute, Moscow.
[6]Johnston Space Center, Houston, Texas.
[7]Goddard Space Flight Center, Greenbelt, Maryland.
[8]Ames Research Center, Moffett Field, California.



Paper number 1999JE001093.
0148-0227/00/1999JE001093$09.00

water-ice clouds and suspended dust, the abundance of water vapor, and the emissivity of the surface materials.

The surface spectra presented here were acquired during the aerobraking phase of MGS and generally have significantly lower quality and lower spatial resolution than is obtained during the mapping phase of the mission. However, even under these less than ideal conditions, the TES spectra present a striking view of the surface of Mars.

## 2. Background

### 2.1. TES Investigation Overview

The specific objectives of the TES experiment are (1) to determine the composition of surface minerals, rocks, and ices; (2) to study the composition, particle size, and spatial and temporal distribution of atmospheric dust; (3) to locate water-ice and $CO_2$ condensate clouds and determine their temperature, height, and condensate abundance; (4) to study the growth, retreat, and total energy balance of the polar cap deposits; (5) to measure the thermophysical properties of the Martian surface materials; and (6) to characterize the thermal structure and dynamics of the atmosphere [*Christensen et al*., 1992].

The TES instrument consists of three subsections: (1) a Michelson interferometric spectrometer, (2) a bolometric thermal radiance (4.5 to ~100 $\mu$m) channel, and (3) a solar reflectance (0.3–2.7 $\mu$m) channel. Data are collected from six ~8.5 mrad instantaneous fields of view (IFOV) in each boresighted instrument subsection during one observation period (2 s). These IFOVs provide a contiguous strip three elements wide with a spatial resolution designed to be 3 km in the final MGS mapping orbit altitude of 350 km. A pointing mirror is used to obtain views of space, an internal reference surface, and the atmosphere above the limb of the planet [*Christensen et al*., 1992]. Observations are time ordered using orbit number (P*n*), which corresponds to one revolution of the spacecraft around Mars, and an incremental counter (ICK) which begins at one on each orbit.

The TES spectrometer has a noise equivalent spectral radiance of $\sim 2.5 \times 10^{-8}$ W cm$^{-2}$ sr$^{-1}$/cm$^{-1}$ from ~300 to 1400 cm$^{-1}$, increasing to $\sim 6 \times 10^{-8}$ W cm$^{-2}$ sr$^{-1}$/cm$^{-1}$ at 250 cm$^{-1}$ and to $\sim 4 \times 10^{-8}$ W cm$^{-2}$ sr$^{-1}$/cm$^{-1}$ at 1650 cm$^{-1}$ [*Christensen*, 1999]. Absolute radiometric accuracy was determined from prelaunch data to be better than $4 \times 10^{-8}$ W cm$^{-2}$ sr$^{-1}$/cm$^{-1}$ [*Christensen*, 1999]. In-flight observations indicate that a small, systematic calibration offset with a magnitude of $\sim 1 \times 10^{-7}$ W·cm$^{-2}$·sr$^{-1}$·cm$^{-1}$ is currently present in the TES data [*Christensen et al*., 1998], but this error is insignificant for the surface observations presented here.

The data discussed in this paper are among the $4.8 \times 10^6$ spectra collected during the aerobraking phase of the MGS mission on orbits P3–P268 (September 14, 1997, through April 29, 1998), corresponding to the Aerobraking Phase 1 (AB1) and Science Phasing Orbit 1 (SPO1) of the MGS mission. These orbits occurred during the southern spring and summer seasons (aerocentric longitude ($L_S$) 182°–319°). Throughout this period the spacecraft was in a highly elliptical orbit, so the spatial resolution and angular velocity varied widely. The spatial resolution during each periapsis pass varied from ~1 km cross-track by ~8 km down-track (due to spacecraft motion) at periapsis to ~15 km at 1500 km altitude. During the aerobraking period the local time of the periapsis varied from 18.5 H (24 H equals one Martian day) to 10 H, and the latitude of periapsis varied from 30° to 70°N. As a result of these viewing conditions, ~75% of the near-periapsis data have surface temperatures between 180 and 240 K, well below the 260–290 K temperature for which the TES was designed to map mineralogy.

The TES aerobraking data were collected under a variety of atmospheric dust conditions, with the infrared opacity varying from typical values of 0.2 to ~1 during a regional dust storm [*Smith et al*., this issue (a)]. This storm occurred from $L_S$ 225° to 270° (orbits P50–P120) and produced dust opacities approaching 1 at its peak near $L_S$ 230° [*Smith et al*., this issue (a)]. This storm had decayed by $L_S$ 270°, and the dust opacity north of 30°S had decreased to less than 0.3 by $L_S$ 260° and remained below this level throughout the aerobraking period. As a result, the SPO1 data on orbits P215–P245 ($L_S$ 304°–312°) were collected under excellent atmospheric observing conditions. The equatorial surface temperature during this period ranged from 260 to 290 K, making the SPO1 data among the best collected during the aerobraking period.

TES spectra are calibrated to radiance using periodic views of space and an internal reference surface [*Christensen*, 1999]. These radiance data are converted to emissivity by (1) deriving the brightness temperature at each wavenumber; (2) finding the maximum brightness temperature over a wavenumber interval from 300 to 1350 cm$^{-1}$ chosen to eliminate points with high instrument noise; (3) setting the maximum brightness temperature equal to the surface kinetic temperature; and (4) computing the emissivity at each wavenumber by dividing by the Planck function at the surface kinetic temperature. This process implicitly assumes that the surface materials have unit emissivity at the point of maximum brightness temperature within the TES spectral range; this assumption has been demonstrated to be valid to within ~3% for a wide range of minerals, rocks, and soils [*Ruff et al*., 1997; *Salisbury et al*., 1991]. Expected temperature variations of 20 K within a single TES pixel can produce a minor curvature across the derived emissivity spectrum that varies from 0.004 at 300 cm$^{-1}$ to 0.008 at 700 cm$^{-1}$ and 0 at 1500 cm$^{-1}$. This minor deviation from a surface with uniform temperature has no effect on the spectral shape derived here.

### 2.2. Previous Studies

**2.2.1. Spectral analyses.** Much of our current understanding of the composition of the Martian surface has been derived from analyses of visible and near-infrared telescopic and orbital spectral observations, along with compositional analyses at the Viking Lander and Mars Pathfinder sites (for reviews, see *Soderblom* [1992], *Roush et al*. [1993], *Bell* [1996], *Banin et al*. [1992], *McSween et al*. [1999], *Bell and Morris* [1999], *Bell et al*. [2000], and *Morris et al*. [2000]).

Reflectance spectra of bright and dark regions on Mars exhibit a ferric absorption edge from ~0.4 to 0.75 $\mu$m, which gives the planet its distinctive color [e.g., *Mustard and Bell*, 1994]. Determining the mineralogical composition of Martian ferric-bearing phases has been a topic of study for many years. The generally featureless shape of the ferric absorption has long been attributed to poorly ordered or amorphous nanophase ferric oxides by analogy with certain palagonitic tephra from Hawaii [e.g., *Evans and Adams*, 1979; *Singer*, 1982; *Adams et al*., 1986; *Morris et al*., 1993; *Bell et al*., 1993; *Morris et*

*al*., 1997]. In the Olympus-Amazonis (bright) region of Mars, the ferric absorption edge has inflections at ~520 and 600 nm, a reflectivity maximum at ~750 nm, and a shallow minimum centered near 860 nm. These features have been associated with subordinate amounts of red (crystalline) hematite compared to the nanophase ferric oxide. *Morris et al*. [1997] reviewed existing laboratory data and suggested that an upper limit of ~5% red hematite was present in Martian bright regions such as Olympus-Amazonis. *Merenyi et al*. [1996] used supervised spectral classification techniques to map spectral units on Mars and identified a large region in Sinus Meridiani as having a relatively high crystalline hematite component. Other bright regions have a shallow minimum near 900 nm [e.g., *Murchie et al*., 1993], implying a ferric oxide other than hematite is present. Goethite, ferrihydrite, jarosite, and schertmannite have all been suggested [e.g., *Murchie et al*., 1993; *Bishop and Murad*, 1996; *Morris et al*., 1996; *Morris and Golden*, 1998].

The infrared interferometric spectrometer (IRIS) on Mariner 9 collected spectral data between 200 and 2000 $cm^{-1}$ (50–5 $\mu$m) during and after the 1971 dust storm at a spectral sampling of 2.4 $cm^{-1}$. These data have been used to study surface composition and have revealed the presence of silicate components on the surface and in the atmospheric dust [*Hunt et al*., 1973; *Christensen*, 1998].

**2.2.2. Lander analyses.** In situ measurements of the Martian soil by the Viking landers in Chryse and Utopia Planitia and by the Pathfinder at Ares Vallis showed strikingly similar bulk elemental compositions and mechanical characteristics, suggesting that the soil may be globally homogenous [*Toulmin et al*., 1977; *Clark et al*., 1982; *Moore et al*., 1977, 1979, 1982; *Reider et al*., 1997]. The soil contains a high amount of Fe relative to terrestrial basalts and an $MgO/Al_2O_3$ ratio close to one [*Banin et al*., 1992]. On the basis of multispectral images (440–1000 nm), rocks and soils at the Mars Pathfinder landing site in Ares Valles can be subdivided into spectral classes on the basis of structure in the ferric absorption edge, the near-IR spectral slope, and the indication of a band in the 800–1000 nm spectral region [*McSween et al*., 1999; *Bell et al*., 2000; *Morris et al*., 2000]. Although there is spectral evidence from the ferric absorption edge that a crystalline ferric oxide (e.g., hematite, goethite, and akaganéite) is present as a minor spectral component, its identity is not known, largely because of the absence of a well-defined band in the 800–1000 nm region. By spectral analogy with certain palagonitic tephra, the optically dominant ferric-bearing phase is poorly crystalline, nanometer-sized particles of ferric oxide dispersed in an aluminosilicate matrix [e.g., *Morris et al*., 1993].

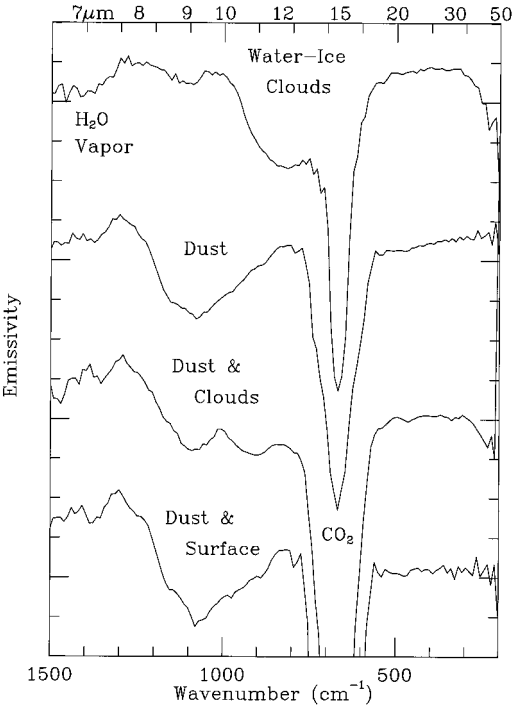


**Figure 1.** Typical TES spectra of $CO_2$, atmospheric dust, water-ice clouds, dust and cloud mixtures, and mixtures of atmospheric and surface components. The "cloud" spectrum was acquired on orbit P48 ($L_S$ 223°), ICK 1118, Detector 1, and is scaled by 50%; the "dust" spectrum is the average of all detectors for ICKs 800–950 on orbit P61 ($L_S$ 234°); the "dust and cloud" spectrum was acquired on orbit P35 ($L_S$ 212°), ICK 1157, Detector 1; the "dust and surface" spectrum is the average of all detectors for ICKs 1663–1675 on orbit P219 ($L_S$ 305°).

## 3. Results

### 3.1. Identification of Unique Surface Spectra

Figure 1 shows representative TES spectra of Mars, illustrating the spectral signatures observed for water vapor, water-ice clouds, atmospheric dust, $CO_2$ gas, and surface materials. In general, the presence of atmospheric constituents necessitates careful analysis in order to isolate the surface components. However, the spectra that are the subject of this paper have features that are readily distinguished from atmospheric features without complex corrections. In particular, the region from 250 to 525 $cm^{-1}$ has spectral features that are distinctly different from the typical Martian atmospheric spectra [*Bandfield et al*., this issue; *Smith et al*., this issue (b)], and provided the means by which these unique spectra were first identified.

The majority of periapsis emissivity spectra have been visually inspected in a search for unique spectral features. The 250–525 $cm^{-1}$ region of most spectra is characterized by high emissivity (>0.9) and a relatively flat or gently sloping continuum with no major absorption features (Figure 1; "dust" spectrum). A few dozen spectra collected in Sinus Meridiani (near 2°S latitude, 3°W longitude) on orbit P222 ($L_S$ 306°) were found to have features that were significantly different from the norm, with distinct emissivity minima at ~450 $cm^{-1}$ and ~300 $cm^{-1}$ and a maximum at ~375 $cm^{-1}$ (Figure 2).

Observations were collected on orbit P133 ($L_S$ 276°) within 25 km of those acquired on orbit P222. These data show excellent agreement in the spatial pattern of spectral properties, despite being separated by 89 orbits (49 days) in time and acquired under different atmospheric conditions, spatial scales, times of day, and emission angles. Given the highly variable nature of atmospheric aerosols [*Smith et al*., this issue (a); J. C. Pearl et al., Mars Global Surveyor Thermal Emission Spectrometer (TES) observations of water-ice clouds during aerobraking and science phasing, submitted to *Journal of Geophysical Research*, 1999], the consistency of these observations demonstrates that these distinctive spectral features arise from surface minerals.

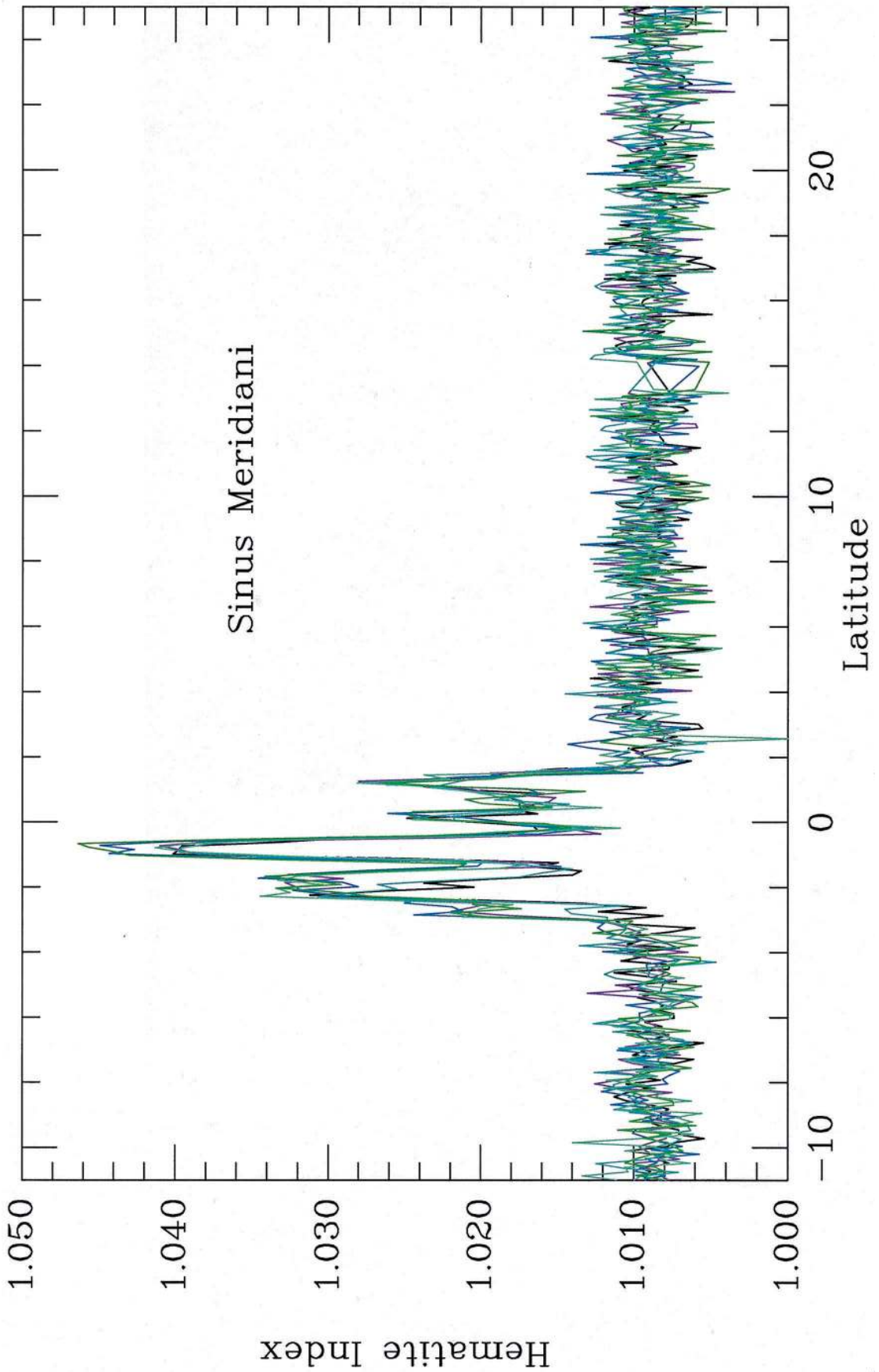


**Plate 1.** Hematite index. Data from orbit P222 for all six TES detectors show a strong hematite signature from 3°S to 2°N. Other portions of this orbit, taken with essentially the same atmospheric and viewing conditions, lack any indication of a hematite signature.

### 3.2. Atmospheric Correction and Noise Analysis

The position and general shape of the prominent absorption bands in the 250–525 $cm^{-1}$ region can be interpreted directly from the emissivity spectra (Figure 2). However, there are several atmospheric absorptions, including water-ice aerosols, water vapor, and atmospheric dust, that influence the specific shape of these prominent bands. Removal of this atmospheric overprint allows for a more precise interpretation of the unknown surface absorptions. A simple radiative-transfer, surface-atmosphere separation technique has been developed that uses a defined spectral dependence of opacity for water ice, atmospheric dust, and $CO_2$ and their retrieved abundances to isolate the surface spectral shape. In this model the contributions of the much weaker water vapor and $CO_2$ hot band absorptions are removed by including their effective opacity in the dust spectral shape.

The spectral shapes of dust and water ice have been defined from several data subsets and have been shown to vary insignificantly with time, space, and view geometry [*Bandfield et al.*, this issue; *Smith et al.*, this issue (b)]. The ice spectral shape was obtained from an average of 39 ICKs collected on orbit P33 ($L_S$ 210°), 51 ICKs on orbit P55 ($L_S$ 229°), and 38 ICKs on orbit P132 ($L_S$ 276°) during periods of heavy ice cloud cover and a relatively low abundance of atmospheric dust [*Smith et al.*, this issue (b)]. The background dust spectral shape has been determined explicitly for orbit P222 using an average of 60 spectra taken from the periapsis of orbit P222 (selected ICKs between 1388 and 1445) from regions within ~150 km of where the unique surface spectral features were observed. Observing conditions (emission angle, surface temperature, atmospheric temperature, dust and ice aerosol amount) were essentially identical for all spectra. The surface-atmosphere separation technique used here assumes that all spectral features in the reference regions result from atmospheric components (i.e., the surface emissivity is unity). As a result, this technique also removes the reference region surface component, which includes a basaltic component [*Christensen et al.*, this issue] that we estimate to cover greater than ~50% of the surface in Sinus Meridiani. This spectral isolation process produces a spectrum that emphasizes the unique component; if this process was applied to two regions containing only the basalt component, the result would be a completely flat spectrum. Thus the isolated spectrum is that of the material that is unique to one of the two regions being compared. In the case of Sinus Meridiani, the distinct spectral features between 250 and 500 $cm^{-1}$ are not observed in the original spectra of the reference regions and are present only in Sinus Meridiani.

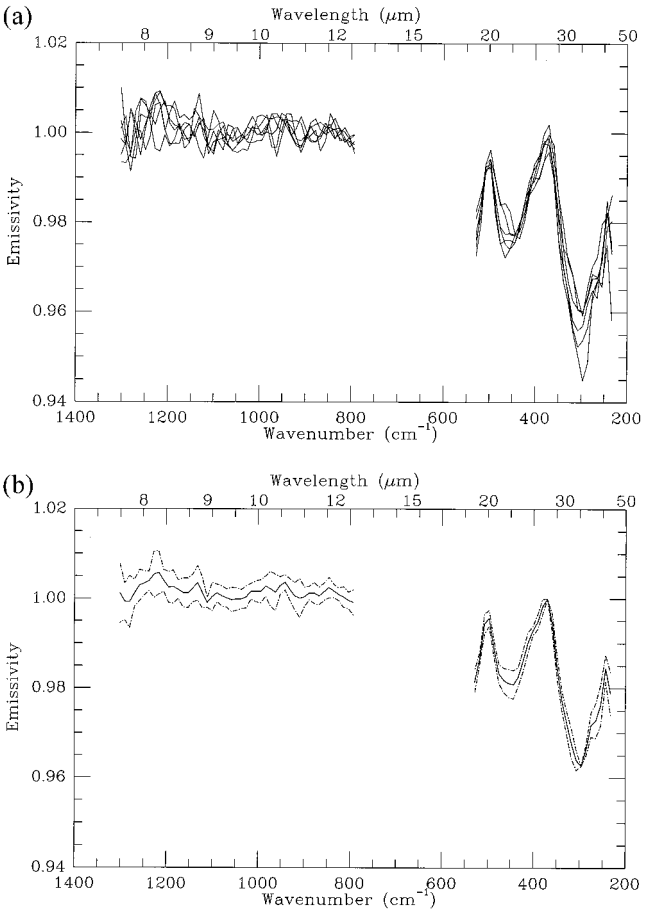


**Figure 3.** Isolated surface component unique to Sinus Meridiani. Atmosphere and average surface components have been removed. (a) Individual surface spectra from all six detectors near 0.8°S, 0.5°W acquired on orbit P222 ($L_S$ 306°), ICK 1407. (b) Average (solid) and normalized $\pm 1\sigma$ variation (dot-dash).

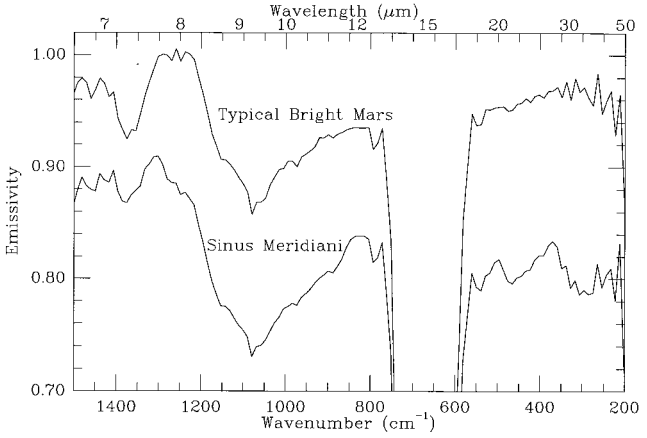


**Figure 2.** Sinus Meridiani spectra and a typical bright-region spectrum. The Sinus Meridiani spectra have distinctive absorption features between 200 and 525 $cm^{-1}$. The Sinus Meridiani spectrum was acquired on orbit P222 ($L_S$ 306°), ICK 1407 (0.8°S, 0.5°W). The "bright region" spectrum is an average of spectra acquired on orbit P219 ($L_S$ 309°), ICKs 1420–1454 between 3.7°N, 208.7°W and 7.7°N, 209.2°W.

The dust and water-ice opacities were determined by performing a least squares fit of the opacity spectral shapes to the TES spectra between 975 and 1200 $cm^{-1}$. The best fit dust opacity was 0.20–0.22 at 1079 $cm^{-1}$ (a nominal low value [*Smith et al.*, this issue (a)]), and the best fit water-ice opacity was consistent with zero to within the estimated uncertainties in the fit. Given these low opacities, scattering is negligible, and the derived opacities of both water ice and atmospheric dust may be removed using a nonscattering model to obtain an isolated spectrum of the unknown surface material. It is not possible to determine the spectral signature of the surface component between 529 and 794 $cm^{-1}$ because of the high opacity of atmospheric $CO_2$.

The spectrum of the isolated Sinus Meridiani component

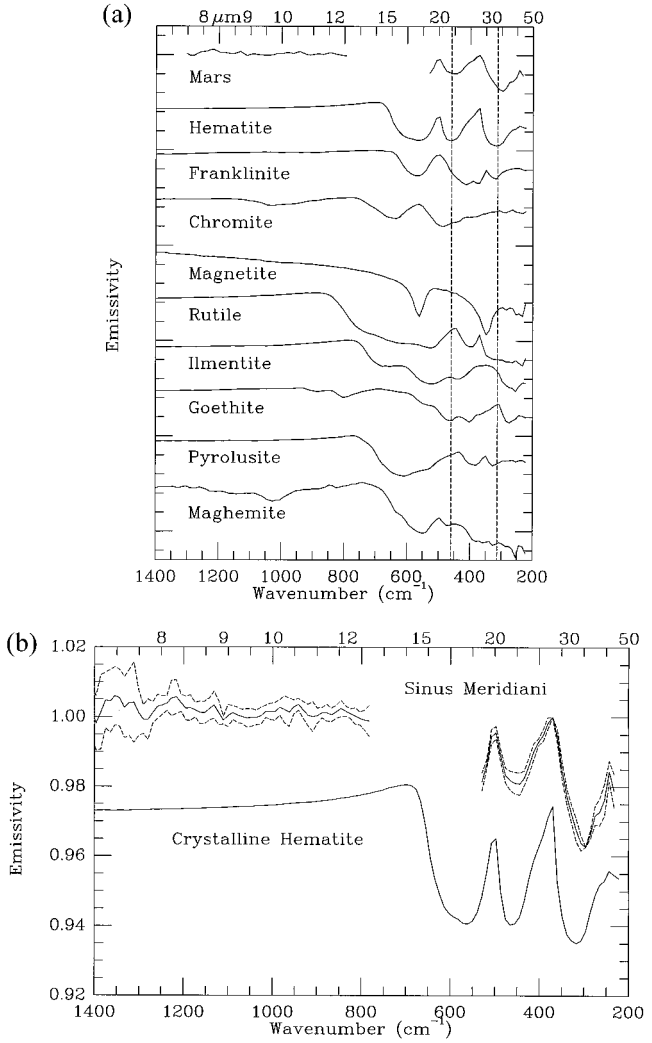


**Figure 4.** Spectra of oxide minerals and oxyhydroxide goethite compared with the average Sinus Meridiani atmosphere-removed and surrounding-area-removed surface spectrum. (a) A suite of minerals measured in emission. Spectra were scaled as indicated and offset by 0.5. The tick mark interval is 0.2. The following spectra have been scaled for clarity: Mars (10×); hematite (0.5×), magnetite (2×), and maghemite (3×). (b) Comparison of the average Sinus Meridiani spectrum and spectra of hematite measured in emission $E$. Note the excellent match, including the minor band at 390 $cm^{-1}$.

with the atmospheric dust and average surface components removed is given in Figure 3. This spectrum is featureless to within the noise level between 765 and 1500 $cm^{-1}$; what remain are three absorption features in the 200–550 $cm^{-1}$ region centered at approximately 300, 450, and >525 $cm^{-1}$.

The TES sample to sample random noise of $\sim 2.5 \times 10^{-8}$ W $cm^{-2}$ $str^{-1}/cm^{-1}$ corresponds to a noise equivalent delta emissivity (NE$\Delta\varepsilon$) of 0.004 at 1000 $cm^{-1}$ and 0.002 at 400 $cm^{-1}$ for the derived surface temperature of the Sinus Meridiani region of 276 K. A separate, more conservative estimate of the uncertainty in the actual shape of the spectral unit was determined using the six spectra acquired simultaneously from each detector on ICK 1407 (Figure 3a). These spectra were normalized at 290 $cm^{-1}$ and 370 $cm^{-1}$ (the maximum and minimum of the deepest band), and the 1$\sigma$ variation was calculated. Obviously, the variation is zero at the points where the spectra are normalized, but for random noise the 1$\sigma$ values away from these points provide a useful indication of the variability. The 1$\sigma$ variation computed in this manner is typically 0.005. Figure 3b gives the average atmosphere-corrected surface spectrum together with $\pm 1\sigma$ values.

### 3.3. Identification of Hematite

Virtually all silicates have major absorptions in the 650–1500 $cm^{-1}$ region that result from the fundamental Si-O stretching vibration [e.g., *Farmer*, 1974]. However, spectra of the isolated Sinus Meridiani component are remarkably featureless in this region, indicating that this component is not a silicate mineral. In contrast, oxide and oxyhydroxide minerals have fundamental vibrational absorption features at longer wavelengths (<800 $cm^{-1}$) that are associated with the metal-oxygen stretching vibration [e.g., *Farmer*, 1974; *Rendon and Serna*, 1981; *Serna et al.*, 1982]. Thus the presence of these features, together with the absence of absorptions in the 650–1500 $cm^{-1}$ region, indicates that the spectrally unique phase in Sinus Meridiani is an oxide.

Figure 4 shows thermal infrared spectra of a suite of oxide and oxyhydroxide minerals collected in emission from 1600 to 200 $cm^{-1}$. These laboratory spectra were acquired using the Arizona State University emission spectroscopy laboratory and have been degraded to TES resolution. The suite of spectra illustrates the variation in the position and shape of the fundamental absorption bands that allows each of these oxide minerals to be readily identified.

The surface spectrum of Sinus Meridiani (Figures 3 and 4b) exhibits three absorption features with minima at approximately 300, 450, and >525 $cm^{-1}$ and maxima at approximately 375 and 500 $cm^{-1}$. These distinct spectral features in crystalline hematite result from the ordered symmetry of the $FeO_6$ octahedra in the mineral. Comparison of the Mars spectrum with the suite of oxide spectra shows that hematite provides an excellent match to both the position and width of the two major absorption bands centered near 300 and 450 $cm^{-1}$ (Figure 4b). Hematite also provides a good match to the position and relative strength of the minor absorption bands at ~390 and 260 $cm^{-1}$. Finally, hematite provides an excellent match to the emission maxima at 375 and 500 $cm^{-1}$. As seen in Figure 4a, none of the other oxides studied provides a match to the Martian spectrum. No other oxide matches the two major absorption features at 300 and 450 $cm^{-1}$, and none of the other oxides matches the detailed band shape, including the position of interband emission maxima, and the position of weaker bands. It is expected, on the basis of similarities in crystal structure, that oxides as a class will have basic similarities in spectral shape. For example, hematite, franklinite, chromite, and magnetite have two major bands in the 300–600 $cm^{-1}$ region. However, it is the precise positions and shapes of the fundamental absorptions that are diagnostic of each specific oxide, and only hematite matches across the entire spectrum. Given the significant differences seen in the spectra of the suite of oxides we studied, we view that it is unlikely that any other oxide would provide as exact a match to the Martian spectra as hematite.

### 3.4. Spatial Mapping

**3.4.1. Hematite index.** In order to map the spatial distribution of hematite, a simple hematite spectral index was developed that measures the depth of the absorption bands near 300 and 450 $cm^{-1}$ relative to the emissivity maximum near 375

$cm^{-1}$ (Figure 3). This parameter is given by $\varepsilon 2/(\varepsilon 1 + \varepsilon 3)$, where $\varepsilon 1$ is the average of TES bands 14 and 15 (band centers at 286–296 $cm^{-1}$); $\varepsilon 2$ is the average of bands 21–24 (360–391 $cm^{-1}$); and $\varepsilon 3$ is the average of bands 31–33 (466–476 $cm^{-1}$). This parameter becomes more positive as the absorption features deepen.

Plate 1 shows an example of the hematite spectral index for orbit P222 over regions with and without a strong hematite spectral signature. The average index value of ~1.009 found between 15°S to 4°S and 3° to 25°N is typical for the vast majority of TES spectra, and variations of ±0.002 are consistent with instrumental noise. The region from 3°S to 2°N has a peak index value that rises above the baseline value by a factor of >15 times the noise level. Inspection of the individual spectra from this region confirms that the spectral signature of hematite can be readily discerned when the hematite index increases above a level of 1.014.

The hematite spectral index was computed for each TES spectrum acquired during the 187 periapsis passes in the MGS aerobraking phase. The data were collected from a spacecraft altitude that varied from ~180 to ~2500 km with an emission angle of <60°, corresponding to spatial resolutions of <70 km and an average TES swath width of ~25 km per orbit. Poleward of ~50°S and ~40°N, the increased noise resulting from low surface temperatures (less than ~205 K) and the presence of significant water-ice opacity make the hematite index unusable; these regions have not been mapped at the present time. These observations cover ~10% of the surface area of Mars in a zone concentrated from 30°S to 30°N. The spacing of orbits at the equator was not controlled but averages to a value of ~115 km.

The hematite index data were examined to search for high values (>1.014) and to eliminate false detections attributable to instrumental noise. All valid hematite identifications during the aerobraking phase occur within the Sinus Meridiani region from 0° to 7°W and 3°S to 2°N. These detections occurred on orbits P47, P77, P123, P133, P136, and P222 between $L_S$ 222° (orbit P47) and 306° (P222) at emission angles of 10° (P222) to 55° (typical) and local times of 15.8 H (P47) to 10.1 H (P222).

On the basis of data from the MGS aerobraking phase we conclude that the Sinus Meridiani region is the only extensive (several hundred kilometer size) occurrence of crystalline hematite within the equatorial region of Mars. An unknown number of smaller accumulations (less than ~150 km in linear dimensions) could be present given the spacing of the aerobraking-phase orbits.

**3.4.2. Sinus Meridiani map.** A map of the hematite index for data from 11 orbits, including the six listed above in which hematite was detected and five orbits that passed nearby, is given in Plate 2. It is apparent from this map that the hematite index successfully detected hematite on all orbits that passed through this region. This consistency provides confidence that the hematite index is a reliable indicator and that equivalent concentrations of hematite do not exist elsewhere in the regions where high-quality TES data were collected.

Plate 2 shows that the boundaries of the hematite-rich region are sharp at spatial scales of ~10 km. Within this region, there are spatial variations in spectral band depth of a factor of 2–3. At the present time the hematite-rich region has not been completely mapped. However, by using the bounding orbits to the east and west in which hematite was not detected, we can establish that this region covers an area that is between 350 and 750 km in length and over ~350 km in width ($1.2 \times 10^5$ to $2.6 \times 10^5$ $km^2$).

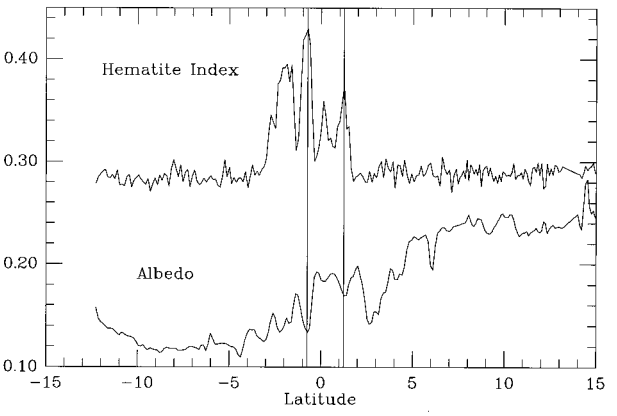


**Figure 5.** Comparison of hematite band depth and surface Lambert albedo. The albedo and hematite index (scaled by (index-0.975) × 10) is shown for Detector 1, orbit P222. The two vertical lines emphasize the correlation between hematite abundance/size and albedo; other correlated locations also exist. Note, however, that the correlation is not exact, with some regions of low albedo not correlated with a higher hematite index.

On the basis of the TES results, *Kirkland et al.* [1999] noted that the Mariner 9 IRIS spectra taken 26 years before the TES observations also show this region to be spectrally anomalous, indicating some stability of the features with time. We have reexamined the IRIS data in Sinus Meridiani collected on orbit 178 ($L_S$ 343°; spacecraft time DAS 7973822, 7973839, and 7974189) and find that the IRIS spectra do show a hematite spectral signature that was not reported in previous studies. A simple ratio of spectra inside and outside (DAS 7973787, 7973804, 7973909, 7973927, and 7973944) the area identified by TES shows an excellent match to laboratory spectra of hematite.

**3.4.3. Correlation with albedo, thermal inertia, and rock abundance.** In addition to providing IR spectral measurements, the TES instrument also contains a visual band that measures reflected solar radiance from 0.3 to 3 μm [*Christensen et al.*, 1992]. Figure 5 shows the spatial variation in hematite index and the Lambert albedo derived from the simultaneous TES solar reflectance measurements. As seen in Figure 5, the spatial variations in hematite band depth and albedo are inversely correlated across the Sinus Meridiani region, with regions of greater band depth being darker than the immediate surroundings. It is important to note that the regions of greatest hematite absorption do not correspond to the darkest regions in Sinus Meridiani (albedo = 0.12); these regions occur farther to the south, where the hematite abundance is low. The observed correlation with albedo is significant because it demonstrates that the hematite is present in sufficient abundance to have a measurable effect on the surface brightness. For regions of highest hematite abundance the presence of hematite lowers the albedo by as much as 0.05.

The thermal inertia in the region of high hematite signature (latitude 3°S to 2°N; longitude 0° to 7°W) measured using high-resolution, predawn Viking infrared thermal mapper (IRTM) data [*Christensen and Moore*, 1992] varies from 5.3 to 10.1 (units of $10^{-3}$ cal $cm^{-2}$ $s^{-1/2}$ $K^{-1}$; 221 to 423 in units of J $m^{-2}$ $s^{-1/2}$ $K^{-1}$), with an average value of 7.4. These values are

only slightly higher than the Martian average value of ~6.5 [*Palluconi and Kieffer*, 1981] and indicate an average particle size of the surface materials of 800–900 μm [*Presley and Christensen*, 1997]. The rock abundance for this area varies from 1 to 13%, with an average value of 7% areal rock cover [*Christensen*, 1986]. These values are typical for much of Mars [*Christensen and Moore*, 1992] but are lower than the values observed at the Viking Lander and Pathfinder sites [*Golombek et al.*, 1999].

## 4. Discussion

### 4.1. Hematite Crystallinity

Hematite occurs in three forms that differ in physicochemical and spectral properties: nanophase, red crystalline, and gray crystalline (specular) hematite [*Morris et al.*, 1985, 1989]. Nanophase hematite consists of X-ray amorphous particles <5–10 nm in size and has neither a well-defined reflectivity maximum near 750 nm nor a well-defined reflectivity minimum near 860 nm in visible/near-IR (VNIR) spectra [*Morris et al.*, 1985, 1989].

Red hematite consists of crystalline (by X-ray diffraction) particles ~10 nm to ~5 μm in diameter. It has well-defined reflectivity maximum and minimum near ~750 and ~860 nm, respectively, and a steep ferric absorption edge in the visible that is responsible for its intense color [*Morris et al.*, 1985, 1989]. (Note that we refer to this type of hematite as red, recognizing that its color can vary from orange to purple). The diameter range for red hematite includes the diameter range for commercial hematite pigments [*Hancock*, 1975; *Morris et al.*, 1985]. Hematite particles larger than ~5 μm (including hematite rocks) can also be red if they are polycrystalline with individual crystallites that are in the diameter range of ~10 nm to 5 μm.

Gray (specular or micaceous) hematite consists of crystalline (by X-ray diffraction) particles >10 μm in diameter or polycrystalline aggregates of those particles. Gray hematite is spectrally neutral (nearly flat reflectivity) at visible wavelengths (400–700 nm) [e.g., *Morris et al.*, 1989].

The degree of crystallinity and particle diameter of the hematite in Sinus Meridiani was investigated by comparing TES emissivity spectra and available Hubble Space Telescope (HST) VNIR multispectral data with corresponding data for nanophase, red, and grey hematite. Figure 6 shows emissivity spectra for powders of red hematite HMS3 (0.14 μm mean particle diameter [*Morris et al.*, 1985]) and nanophase hematite TNA30-215 (similar to TNA13-210 [*Morris et al.*, 1991]). As seen in Figure 6, the nanophase sample does not show well-developed absorption bands above the noise level in the 450–700 $cm^{-1}$ region. In contrast, even though the red hematite is extremely fine grained, which results in low spectral contrast, it still exhibits discernable absorption features at 450 and 550 $cm^{-1}$. Coarser-grained samples show much stronger 450 and 550 $cm^{-1}$ bands (Figure 4).

On the basis of comparison of TES and laboratory data we conclude that the hematite in Sinus Meridiani has an ordered symmetry of the $FeO_6$ octahedra and is either red or gray, but not nanophase, hematite. The HST data do not show a strong band depth at ~530 nm (an indicator for red hematite) in the Sinus Meridiani hematitic region relative to the surrounding areas [*Bell and Morris*, 1999]. If the absorptions observed by TES were produced by red, fine-grained hematite, then HST would show a brilliant signature of red hematite. Instead, the HST data do not show obvious evidence for an unusual abundance of red hematite in the region observed by TES. Therefore, although we cannot exclude the presence of red hematite in Sinus Meridiani, our preferred interpretation based on the arguments developed above is gray hematite with particle diameters >5–10 μm.

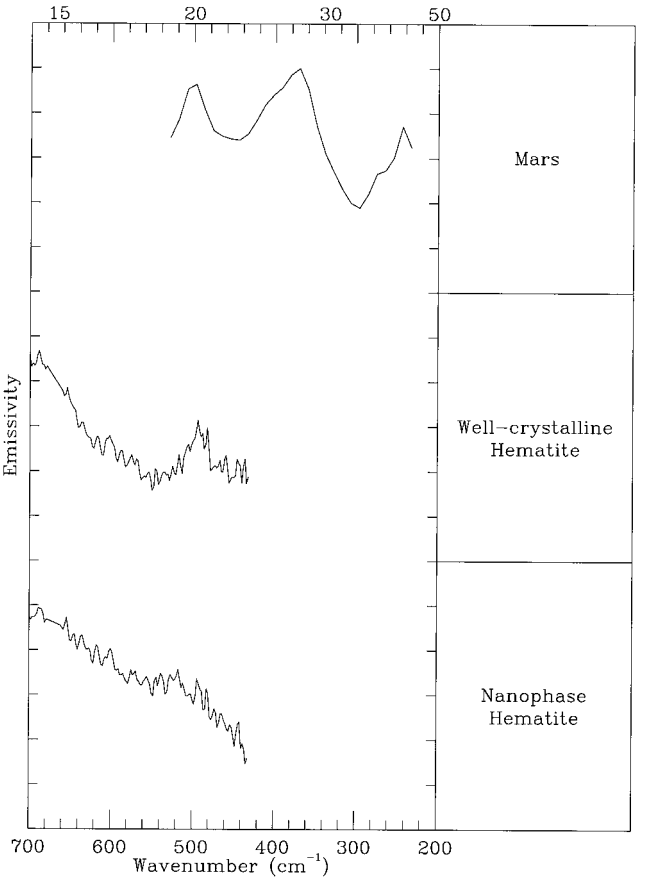


**Figure 6.** Averaged Sinus Meridiani spectrum compared to spectra of fine-particulate crystalline (<0.14 μm, red) and nanophase (greater than ~10 nm) hematite samples. The nanophase sample lacks any indication of the band at 450 and >525 $cm^{-1}$.

### 4.2. Particle Size and Packing

As particle dimensions approach the wavelength of observation, their size and packing can affect both the depth and shape of infrared spectral bands, providing additional insight into the physical properties of Sinus Meridiani hematite [*Vincent and Hunt*, 1968; *Hunt and Logan*, 1972; *Hapke*, 1993; *Salisbury and Eastes*, 1985; *Moersch and Christensen*, 1995]. Figure 7 shows the variation in hematite spectra with particle diameter for size separates obtained by grinding and sieving a hand specimen of gray hematite. As expected, the strong fundamental bands in the 200–700 $cm^{-1}$ region show no variation in depth with particle size for particle diameters >30 μm, but the band depths do decrease for particles <20 μm.

The shapes of fundamental spectral bands of the hematite particle-size series were matched to the TES spectrum using the modified least squares feature fitting algorithm of *Clark et al.* [1990], in which the weighting in the weighted fit is by the relative area of each feature. A feature by feature comparison

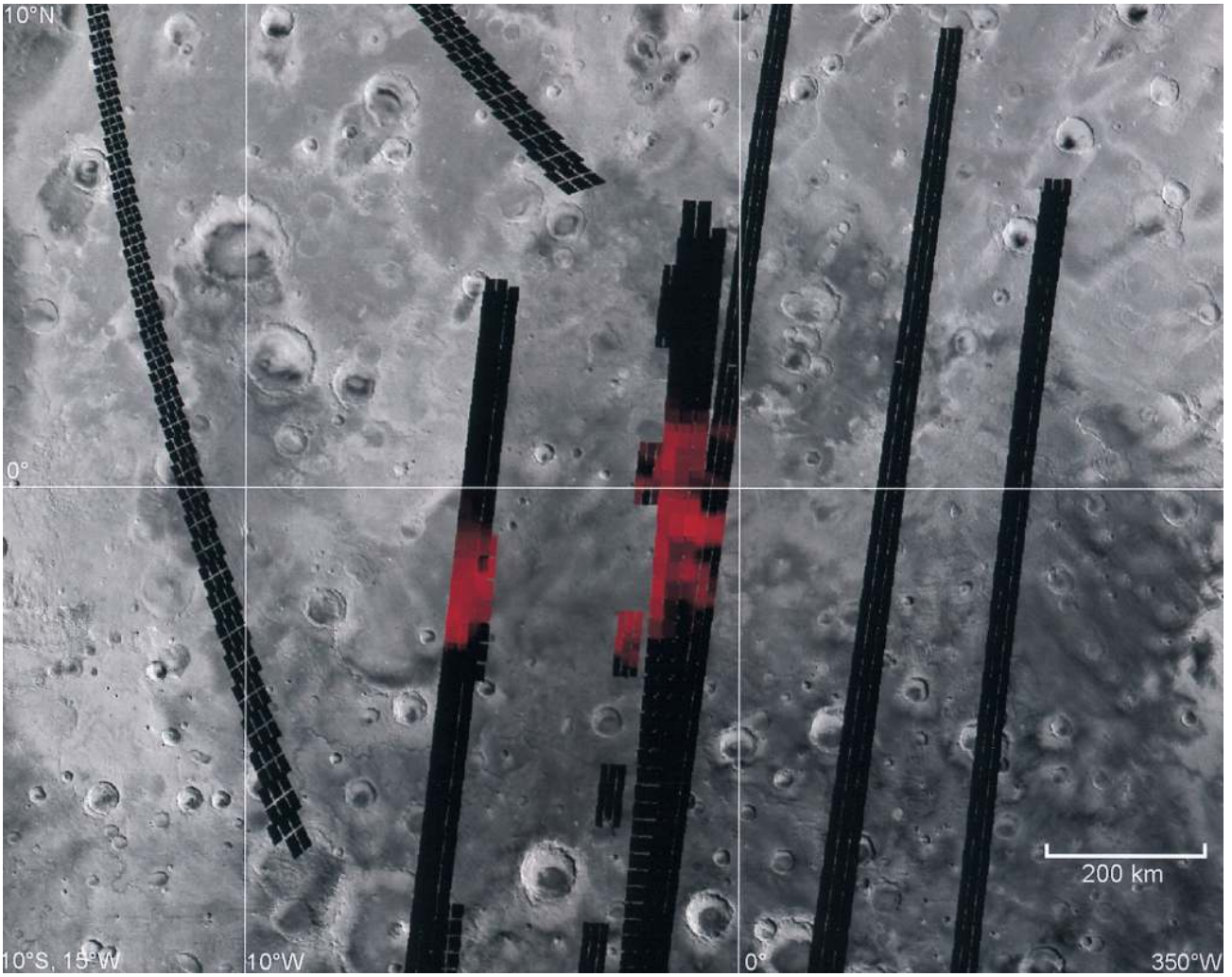


**Plate 2.** Hematite distribution map showing the concentration of hematite measured by the TES instrument. The magnitude of the hematite index is shown in red from 1.010 (black) to 1.045 (saturated red). The location and size of the individual TES observations on the surface are indicated by the individual squares. Black squares indicate observations with no detectable hematite. Data from 11 separate orbits acquired between November 22, 1997, and April 25, 1998, are shown in this image. The TES data are superimposed on a Viking photomosaic for context.

gives a best fit to 10 $\mu$m particles, although all particle sizes give an acceptable fit and much coarser particles cannot be excluded.

For small particles, multiple scattering becomes important, and the path length of emitted energy through the material increases significantly [*Vincent and Hunt*, 1968; *Hunt and Logan*, 1972; *Hapke*, 1993; *Salisbury and Eastes*, 1985; *Moersch and Christensen*, 1995; *Lane*, 1999]. As a result, weak absorptions, minor contaminants, and adsorbed water can increase the true absorption and cause a decrease in emittance. This effect has become known as a transparency band and is observed in the $>700$ cm$^{-1}$ ($<14$ $\mu$m) spectral region in hematite for particle sizes $<100$ $\mu$m (Figure 7). However, in natural samples containing absorbers in the region of these weak bands (such as silicates in the case of hematite) these transparency effects are typically not observed [*Clark and Lucey*, 1984], and the presence or absence of the weak bands at $>700$ cm$^{-1}$ is not diagnostic of the particle diameter of Sinus Meridiani hematite.

Packing can have a significant effect on thermal IR spectra when the particle size is similar to or less than the wavelength of observation. While a loose powder surface, typical of windblown dust, will show multiple scattering in regions of spectral transparency, a packed or cemented surface will behave more like a single large particle. Figure 7 illustrates the effect of packing on band depth in hematite. In an unpacked powder of submicron red hematite, the fundamental bands in the 200–700 cm$^{-1}$ region have low spectral contrast ($\varepsilon > 0.95$). When that same powder is hand packed, the depths of these bands increase by a factor of 10, the effect of multiple scattering is significantly reduced, and the band depths mimic those of coarser particles.

The spectral shapes of the hematite fundamental bands in packed particles, however, do not match those of coarser particles. Scaled spectra for packed and unpacked fine particulate hematite samples are compared in Plate 3, in which we have isolated the spectral shape of hematite by scaling the band depths separately to a common intensity (or area). The positions and shapes of the bands centered at 300 and 450 cm$^{-1}$ show little variation with packing for submicron particles. Thus

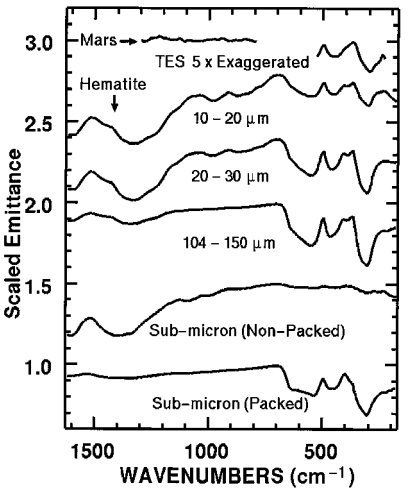


**Figure 7.** Spectra of hematite as a function of particle diameter and packing. As the particle size decreases, the fundamental region spectral structure remains relatively constant to particle sizes <20 μm. At high wavenumbers, spectral structure increases with decreasing particle size because of water adsorbed onto mineral grains, the transparent nature of hematite, and the presence of minor contaminants. The variation in band depth with packing is illustrated using submicron particles both unpacked and packed with a pressure of 1 kg $cm^{-2}$. The band depths deepen with packing, and multiple scattering at high wavenumbers is reduced, but band shape does not vary. Spectra were measured at the U.S. Geological Survey Denver in reflectance and converted to emittance using Emittance = 1 − Reflectance.

the spectral shape of submicron particles (packed or unpacked) is unique and differs from coarser grains by more than the uncertainty in the TES spectra (Figure 3b). We therefore conclude that submicron hematite powders (both packed and unpacked) can be excluded as good fits to the TES data.

Examination of the spectral properties of other hematite samples shows minor variations that further complicate the precise determination of particle size. We therefore conclude that Sinus Meridiani hematite detected by TES is composed of particles at least 10 μm in size that could be sand sized or larger. Packed (or cemented) grains could be present, but even packed grains must be >10 μm in size. As discussed in section 4.1, HST VNIR multispectral data [*Bell and Morris*, 1999] suggest that Sinus Meridiani hematite is gray hematite and is therefore not unpacked or packed red hematite. Thus we again conclude that Sinus Meridiani detected by TES hematite has particle diameters >5–10 μm, is gray, and does not contribute a red component to the color of the hematitic Sinus Meridiani region.

### 4.3. Hematite Abundance

Because of the variation in the depth of the hematite fundamental vibrations with particle size, the amount of hematite on the surface in Sinus Meridiani can be estimated only as a function of particle size. We have determined the areal fraction of hematite that would be required to match the observed band depths (Figure 3) using the variation in band depth with particle size for two different hematite samples and both the 300 and 450 $cm^{-1}$ bands. The results are shown in Plate 4. For particles >30 μm, ~10% of the surface would need to be covered by hematite in order to produce the observed band depths. The required abundance increases to 20–30% for 10–20 μm particles and to ~25–60% for particles <10 μm in size. For packed or cemented grains the hematite abundance would be less than for unpacked grains but would still be >10% (Plate 4). Analysis of the full TES spectra indicates that an additional basaltic component with an abundance of >50% is required to match the 8–14 μm region of the spectrum (section 3.2.) [*Christensen et al.*, this issue]. The hematite abundance for >10 μm particles of gray hematite, which is our preferred interpretation as discussed above, can be easily accommodated with this basaltic component. Estimated hematite abundances for <10 μm particles, however, are unrealistically large, supporting the argument that nanophase and red hema-

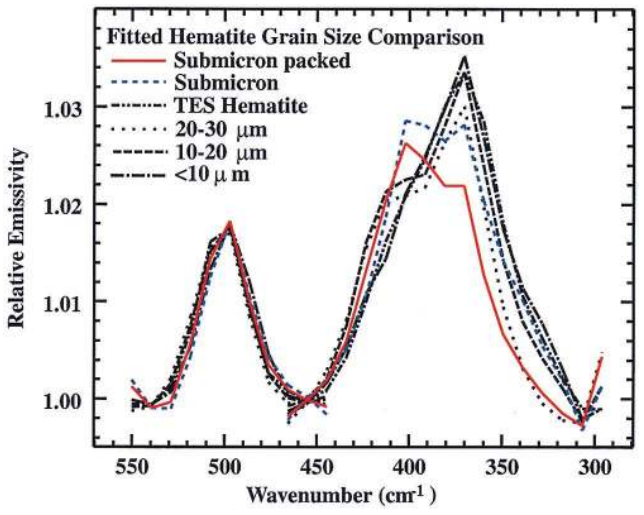


**Plate 3.** The effect of packing on spectral shape. Scaled spectral feature shapes for a suite of hematite grain sizes and packing are compared to the measured TES spectrum. The spectra of submicron grains do not change shape with packing, are unlike those of larger particle sizes, and do not provide a good match to the TES data.

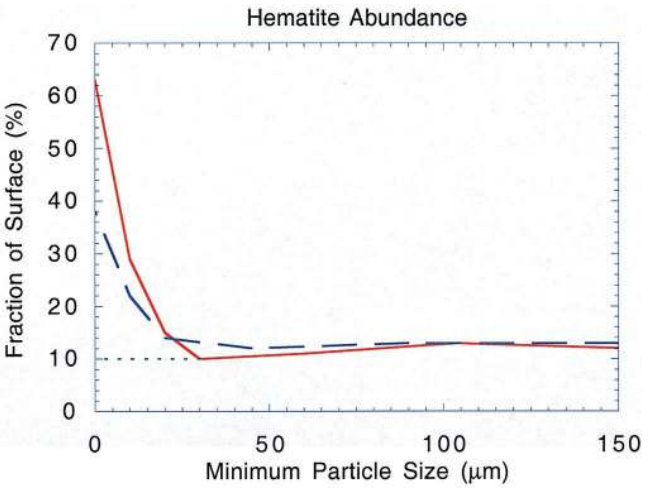


**Plate 4.** Hematite abundance in Sinus Meridiani versus particle size. The depth of the hematite bands at 300 and 450 $cm^{-1}$ was used with particle size suites from two hematite samples (GDS69 (solid line) and HMIR2 (dashed line)) to determine the fraction of the surface covered by hematite for different particle sizes. The dotted line represents the lower limit for packed fine (<10 μm) particles.

tite are not the cause of the spectral signature observed in emissivity spectra of Sinus Meridiani.

### 4.4. Sinus Meridiani Geology

**4.4.1. Regional context and geomorphic provinces.** The hematite-rich surface is located within the classical low-albedo (albedo <0.15) region of Sinus Meridiani (7°N to 13°S; 350°W to 10°W). This area has been observed for more than 350 years [*Antoniadi*, 1930] to be one of the most persistent low-albedo regions on Mars. The low-albedo surface materials are superposed on a substrate that ranges in geomorphic expression from eroded, layered units in northern Sinus Meridiani to more heavily cratered surfaces both to the south and to the north.

Figure 8 shows a simplified sketch map of the general geomorphic units in the Sinus Meridiani region. The units portrayed here are not the same as the previously published, global maps of *Scott and Tanaka* [1986] and *Greeley and Guest* [1987]; instead, the units represent a refinement based on mapping efforts begun by *Edgett and Parker* [1997]. As noted by *Edgett and Parker* [1997], the heavily cratered unit in southern Sinus Meridiani ("ch" in their map, "hc" in Figure 8) contains features that are typical of the Martian southern highlands: ancient, eroded impact craters and a variety of branching, valley network troughs and valleys. MGS Mars Orbiter Camera (MOC) images have shown that unit hc is overlain by a smooth-surfaced (at meter scales), low-albedo mantle that varies in thickness up to several meters (e.g., MOC image AB-1-030/02 [see also *Edgett*, 1999]). Unit bc, to the north, is similar to hc but generally has fewer valley networks and exhibits many small mesas, buttes, and yardangs etched into the cratered surface, suggesting that an overlying material has been largely removed via aeolian deflation [*Presley*, 1986; *Edgett and Parker*, 1997].

Between the heavily cratered units lies a series of eroded, layered materials that have been subdivided here into two geomorphic units: sm (smooth surface) and br (bright and rough surface; Figure 8). Unit sm is characterized by a relatively smooth, layered surface as seen at the limit of Viking Orbiter image resolution (~30 m pixel$^{-1}$). Ring-shaped hills are interpreted to be impact craters rims that have been exposed by erosion from beneath sm (Figure 8). Unit sm is bounded on its western edge by a cliff that exhibits exposed layers or terraces (Figure 9b), and it has a few mesas superposed on it in the southwestern portion of the unit (Figure 9c).

Unit br has a generally rough surface with outcrops of bright and dark materials that appear to be layered and in various states of erosion and exposure [*Presley*, 1986; *Murchie et al*., 1993]. The north and east margins of br have cliffs with exposed layers that appear to be horizontal in ~10 m pixel$^{-1}$ MOC images (e.g., SPO-2-389/03). The regional slope [*U.S. Geological Survey*, 1991] is toward the north and west; thus sm is probably both topographically and stratigraphically higher than br.

The northern boundary of the hematite-rich region in the north (Plate 2) closely matches the location of the contact between sm and br. Similarly, the southern edge of the hematite-rich surface corresponds to contact between sm and hc. Despite significant aeolian activity in this region, the hematite does not appear to have been transported away from or into sm. We therefore conclude that the hematite originates in unit sm.

Prior to the TES discovery, these layered units were variously interpreted as (1) a stripped aeolian deposit and/or volcanic plain and/or cratered terrain [*Scott and Tanaka*, 1986; *Greeley and Guest*, 1987]; (2) a paleopolar deposit that indicated "polar wandering" on Mars [*Schultz and Lutz*, 1988]; or (3) a wind-eroded, ancient, subaqueous sedimentary deposit [*Edgett and Parker*, 1997].

**4.4.2. Physical characteristics of the hematite-bearing smooth unit ("sm").** On orbit P77 (December 29, 1997; $L_S$ 246°) the MOC and TES instruments obtained simultaneous observations of the hematite-bearing surface. The MOC image (AB-1-077/04; Figure 10) covers an area 9 km wide by 95 km long at an apparent resolution of ~20 m pixel$^{-1}$. The image crosses the contact between the smooth (sm) and heavily cratered (hc) units shown in Figure 8, which is also the contact between hematite-rich and hematite-poor surfaces. Figure 10a shows a typical view of the smooth-surfaced unit (sm) as it appears in a subframe of MOC image AB-1-077/04 and confirms that this surface is relatively smooth at 20 m scales. Small, rimless, bowl-shaped depressions are interpreted to be the remains of impact craters with ejecta deposits and rims that have been largely destroyed by erosion of the upper surface. The large ridge in the top right corner of Figure 10a is the rim of a 19 km diameter, partly eroded and exhumed impact crater. We interpret the dark, smooth material in this image to be a surface cover that obscures an underlying, relatively bright material into which are set the bowl-shaped depressions.

Figure 10b shows the contact between the smooth unit (sm) and the cratered and channeled unit (hc) of southern Sinus Meridiani. The TES observations taken simultaneously show that the crystalline hematite is absent on the terrain that lies immediately south of this contact. The ridges on hc represent topographic highs located between the mouths of channels that terminate at this contact. There is no evidence that these channels extend into sm, and sm appears to stand above, and possible embay, the floor of these channels. The edge of sm exhibits a set of parallel ridges and troughs that run along the contact between the two units and mimic the planimetric expression of this contact.

**4.4.3. Interpretation.** Because the hematite-rich surface discovered by TES closely corresponds with smooth-surfaced unit sm, the formation of the hematite-bearing material is intimately linked to the formation of this unit. Unit sm appears to be the surface of a layered sequence. The presence of small mesas superposed on unit sm and the degraded nature of the small impact craters suggest that stratigraphically higher material has been removed from the area to expose or produce the sm surface. It is thus possible that the hematite originated in a stratigraphically higher layer and is now exposed as a lag.

Unit sm appears to be stratigraphically above the old cratered terrain to the north (unit bc), yet in places it appears to be topographically below, and/or possibly embay, the heavily cratered unit to the south (hc). Our observations also suggest that sm appears to overlie the bright, rough unit, br, which in turn overlies bc. The stratigraphic position of unit sm relative to the cratered terrain (hc) in southern Sinus Meridiani is less certain. There are two possibilities: (1) hc is the same surface as bc, and sm is stratigraphically above both of the units (Figure 11a), or (2) hc is stratigraphically higher than unit sm, and sm is a layer within the heavily cratered materials (Figure 11b).

Neither the images taken by the Viking Orbiters nor MOC image AB-1-077/04 (Figure 10) provide conclusive information about the relative position of hc and sm. *Edgett and Parker* [1997] argued that sm covers older hc material on the basis of

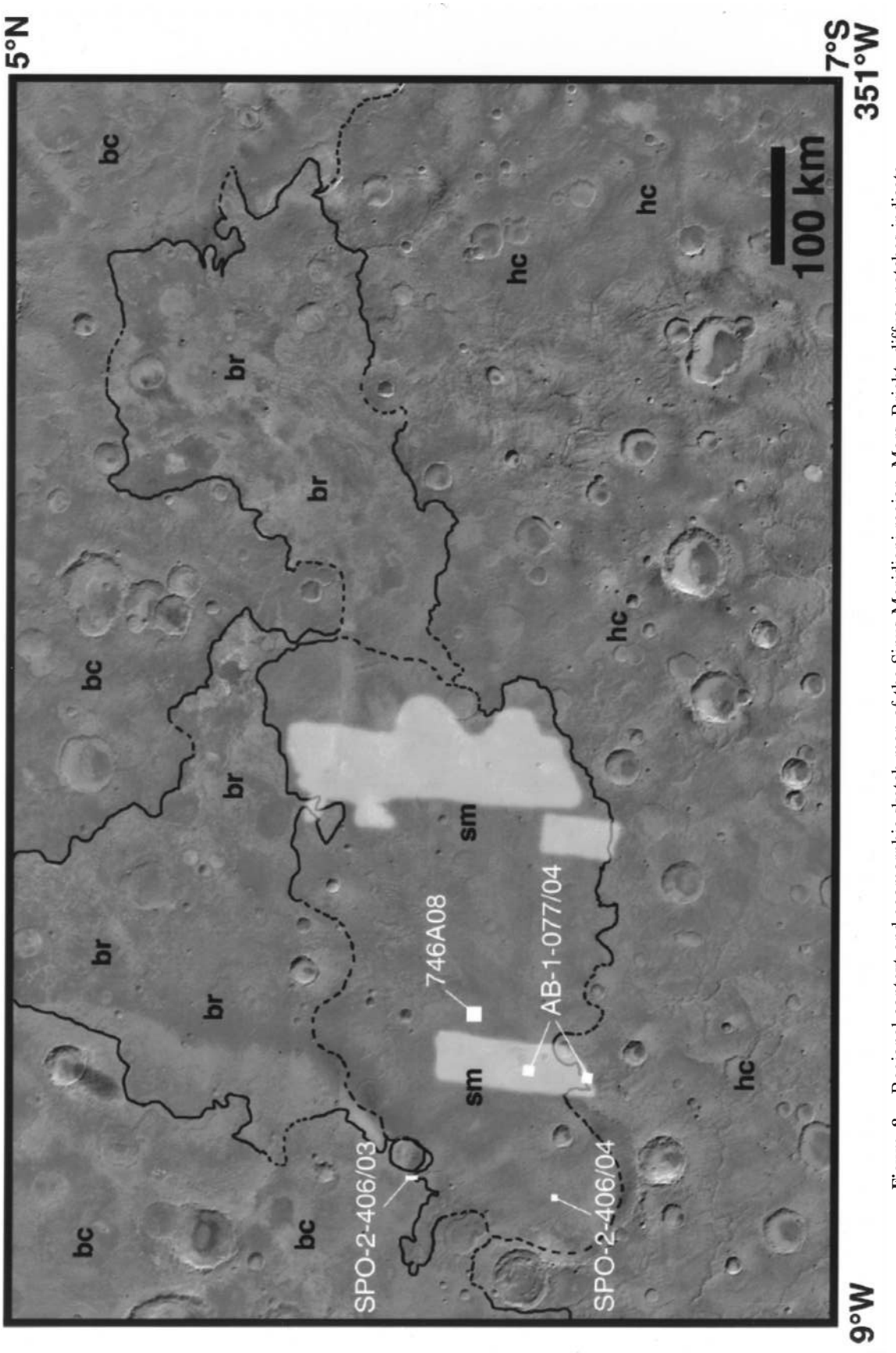


**Figure 8.** Regional context and geomorphic sketch map of the Sinus Meridiani region, Mars. Bright, diffuse patches indicate the location of crystalline hematite as seen by MGS TES (see Plate 2). The geomorphic units (contacts are dashed where placement is less certain) are described in the text. Unit labels indicate the following: hc, heavily cratered surface; bc, buttes and cratered surface; br, bright and rough surface; and sm, smooth surface. White boxes indicate the size and location of MGS Mars Orbiting Camera (MOC) and Viking Orbiter images (labeled by image identification number) shown in Figures 9 and 10. The base map is a simple cylindrical projection of the U.S. Geological Survey Mars Digital Image Mosaic (MDIM) compiled from Viking orbiter images.

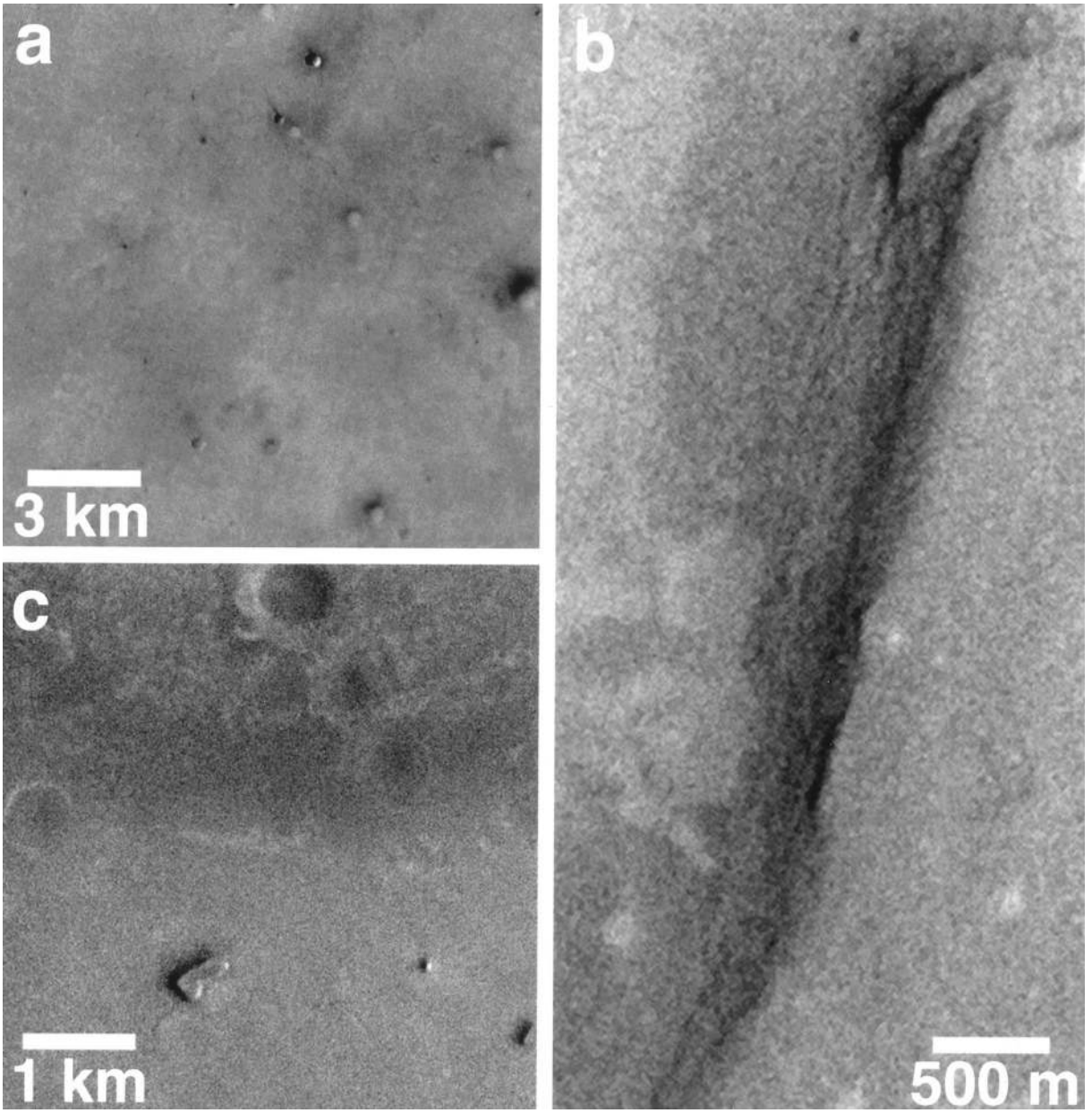


**Figure 9.** Geomorphic features that characterize the smooth-surfaced unit sm. (a) Subframe of Viking Orbiter image 746A08 showing the general character of the sm unit. This image shows a relatively smooth surface with occasional shallow, bowl-shaped depressions interpreted to be eroded impact craters, plus three more recent impact craters (not as severely eroded) in the top center of the frame. North is up; illumination is from the left. (b) Subframe of MGS MOC image SPO-2-406/03 showing the western margin of the sm unit. This margin is a cliff that exhibits layers or terraces on its slope. The smooth (sm) surface is on the right; the lowland to the left is mapped as unit bc. North is up; illumination is from the bottom right. (c) Subframe of MGS MOC image SPO-2-406/04, showing three subkilometer-sized mesas that are superposed on unit sm. Note the shallow, bowl-shaped depressions in the top half of the frame; these are similar to the depressions in Figure 9a. North is up; illumination is from the bottom right.

the indication from Viking Orbiter images (408B27–30) that sm embayed hc and was therefore younger. MOC image AB-1-077/04 may also indicate that sm overlies hc because (1) there is no evidence for the expression of the channel carved in hc in the sm unit; (2) sm appears to be topographically above and embay the floor of this channel in hc; and (3) there is no evidence for the remains of large, eroded impact craters on sm. It seems less likely that large, degraded craters would be present both above (hc) and below (bc) but be absent on sm if sm is a layer between these cratered surfaces. Together, these observations suggest that sm mantles hc.

The ridges in sm that parallel the contact between sm and hc (Figure 10b) suggest a relationship to this contact. If sm is stratigraphically above hc, these ridges could have been formed by a variety of processes related to the emplacement of sm or its subsequent erosion or modification. Alternatively, these landforms could be successive ridges of more resistant material that were left behind as hc retreated via some erosive

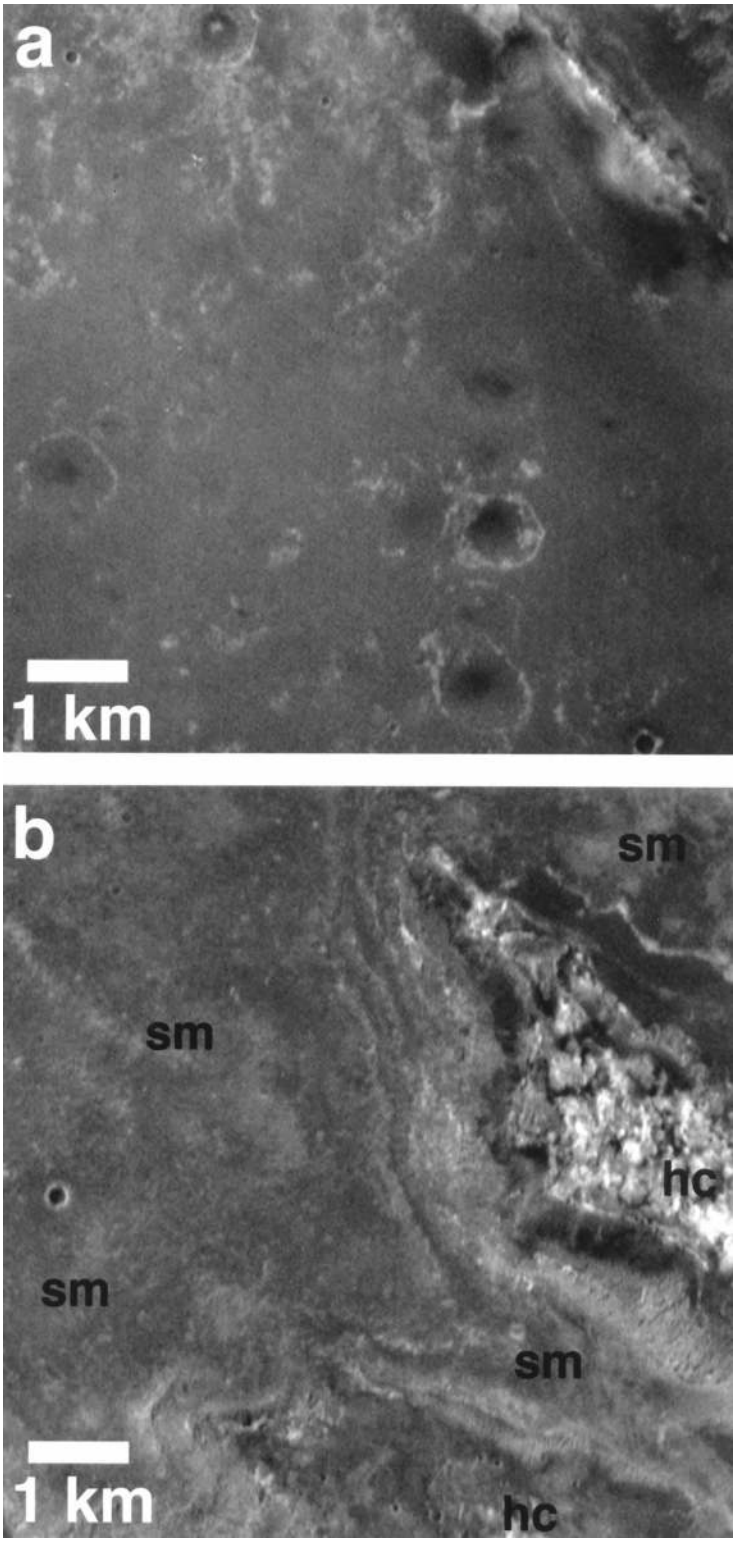


**Figure 10.** Two subframes of MGS MOC image AB-1-077/04, taken simultaneously with TES observations of hematite in December 1997. In both images, north is up, and illumination is from the lower left. Note the location and context of each image in Figure 8. (a) Sample of the hematite-bearing surface. The ridge in the top right is the rim of a partly eroded and partly exhumed impact crater. The smooth, dark surface appears to overlie a brighter and perhaps rougher surface. The bowl-shaped depressions with bright rims are interpreted to be small impact craters that formed in the underlying bright material; the crater rims and ejecta have been removed by erosion. The image appears to indicate a surface that has undergone aeolian deflation. (b) A high-resolution view of the contact between the smooth unit (sm) of northern Sinus Meridiani and the heavily cratered unit (hc) of southern Sinus Meridiani. The contact includes a series of parallel ridges and troughs that might be related to the erosion of the smooth unit or scarp retreat of the cratered unit. No hematite was found to occur south of this contact.

process, suggesting that sm is a layer between bc and hc. A third possibility is that these ridges represent the termini of the ejecta blanket of an old impact crater located to the west of the MOC image.

Regardless of the stratigraphic position of sm, the hematite appears to be intimately associated with layered geologic materials. These layered materials do not appear to be primary volcanic products (i.e., lava flows) because there are no associated lava flow lobes, fronts, or pressure ridges; there are no fissures or calderae or any other features that can be interpreted as being volcanic within sm. In addition, the bowl-shaped depressions in sm (Figure 10a) and the remnant mesas on top of a portion of this unit (Figure 9c) suggest that deflation has removed material that was once above the present surface of sm. The most likely cause of the deflation is wind, which suggests that the layered materials are relatively friable. Deflation of the layered material in northern Sinus Meridiani is consistent with the presence of thick mantles and aeolian bed forms covering the craters and valleys of southern Sinus Meridiani [*Edgett*, 1997].

In summary, the hematite appears to have originated from layered materials that are most likely part of a friable, sedimentary unit. Sources for fragments that comprise these sedimentary units include aeolian, and perhaps fluvial, erosion and deposition of volcanic and other crustal rocks, subaerial and/or subaqueous deposition of explosive volcanic materials, meteor impact, and chemical precipitation.

### 4.5. Possible Origins for Sinus Meridiani Hematite

The high crystallinity, large particle size (>10 $\mu$m), gray color, high abundance, correlation with layered units, and localized occurrence of the hematite exposed in Sinus Meridiani indicate that the oxide was formed by a sequence of events that did not occur ubiquitously on the planet. Below, we discuss possible formation mechanisms for the crystalline gray hematite. With one exception these mechanisms require the occurrence of a significant amount of near-surface liquid water, which has major implications for the evolution of Mars.

The five formation mechanisms for the Sinus Meridiani crystalline hematite that we consider can be grouped into two classes: first, chemical precipitation that includes origin by (1) precipitation from standing, oxygenated, Fe-rich water (oxide iron formations), (2) precipitation from Fe-rich hydrothermal fluids, (3) low-temperature dissolution and precipitation through mobile ground water leaching, and (4) formation of surface coatings, and, second, thermal oxidation of magnetite-rich lavas.

**4.5.1. Oxide iron formations: Direct precipitation from oxygenated, Fe-rich water.** *Burns* [1993] originally proposed, and *Schaefer* [1996] and *Calvin* [1998] pursued, the possible development of banded iron formations (BIFs) (alternating layers of silica-rich and iron-rich bands) on Mars that are analogous to those formed on the Earth during the Archean. They suggested that large amounts of ferrous iron were dissolved into acidic and anoxic ancient Martian seas and subsequently precipitated as insoluble hydrous ferric oxides when the upper layers of the seas became oxygenated. *Morris* [1993] explained the banded nature of the Hamersley (Australia) BIFs by silica-saturated surface waters (source of silica gel or chert) which were periodically overwhelmed by deeper, ferrous-rich water (source of hydrous ferric oxides) during convective upwelling in association with mid-ocean ridges or local hot spots. Metamorphism (by burial) of these chemical precipitates produced coarsely crystalline materials like gray hematite, magnetite, and quartz. The emissivity spectrum of a Brazilian itabirite (a Precambrian BIF from the Quadrilatero Ferrifero, Minas Gerias State, Brazil [e.g., *Curi and Franzmeier*, 1987; *Ramanaidou et al*., 1996]) clearly shows the presence of both hematite and quartz (Figure 12).

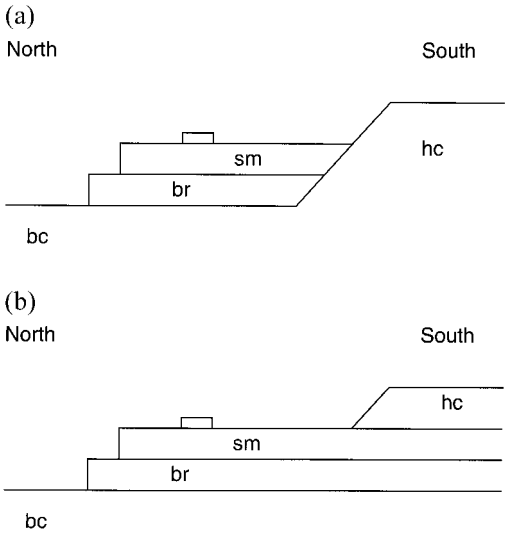


**Figure 11.** Stratigraphic relationships of unit hc: (a) possible model in which sm and br overlie hc and (b) possible model in which sm occurs as a layer between hc and bc.

The TES data of the Sinus Meridiani region, however, show no evidence of either chert or quartz. Quartz is not detected in the original, uncorrected spectra of this region, nor is it found in the basaltic component at abundances of ~5% [*Christensen et al*., this issue]. If the hematite is from a BIF-like process, the absence of the silica-rich phase requires explanation. In a recent study, *Powell et al*. [1999] suggested that silica was removed and giant ore bodies of microplaty hematite formed from the Hamersley BIFs by invasion of hot fluids (200°–400°C) associated with orogeny. Another example, which is associated with volcanism, is the El Laco magnetite/hematite flow in northern Chile [*Park*, 1961; *Frutos and Oyarzun*, 1975]. According to *Frutos and Oyarzun* [1975], the magnetite/hematite flows result from remobilization of sedimentary iron oxides from deeply buried BIFs. It is also possible that the deposition of silica did not occur on Mars because of a unique set of pH and oxidation conditions.

The primary arguments against this model include (1) the apparent absence of quartz and (2) the requirement of large, contained body of liquid (but possibly ice-covered) water. Several mechanisms to account for the absence of quartz were discussed above. *Edgett and Parker* [1997] have presented arguments that unit sm was deposited in liquid water based on the observation that this unit embays and is topographically lower than the hc unit to the south. To the north, sm appears to be topographically higher than bc, suggesting that water would have had to cover a substantial area [*Edgett and Parker*, 1997].

**4.5.2. Precipitation from Fe-rich hydrothermal fluids.** Coarse-grained, gray hematite can form in hydrothermal systems involving large amounts of hot water moving through iron-bearing rocks. The solubility of Fe in water varies with temperature and pressure, causing Fe to be dissolved, trans-

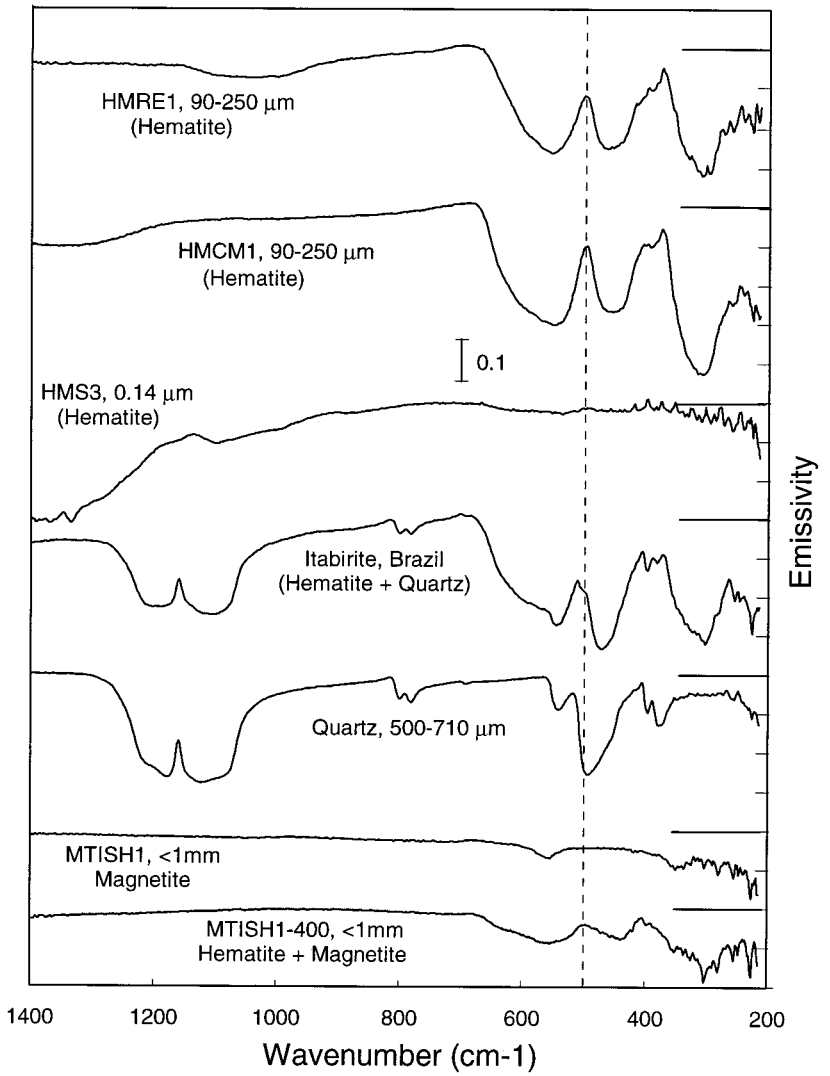


**Figure 12.** Emission spectra of hematite rock and powder samples. A Precambrian banded iron formation itabirite from the Quadrilatero Ferrifero, Minas Gerias State, Brazil, is shown compared with a quartz spectrum. Both quartz and hematite are clearly evident in this sample. Spectra of red (kidney ore from Cleator Moor, Cumberland, England) and gray (Republic, Michigan), crystalline hematite are shown for 90–250 $\mu$m powders. Both red and gray samples show distinct absorption bands from 250 to 550 $cm^{-1}$. Nanophase hematite is also shown, illustrating the absence of bands in the 250–550 $cm^{-1}$ region. The effect of converting magnetite powders to hematite by heating in air is illustrated. The magnetite fundamental vibration at ~550 $cm^{-1}$ is clearly visible in the unheated sample, whereas the spectrum of the heated sample is dominated by the two hematite fundamental vibrations at 450 and 525 $cm^{-1}$.

ported, and precipitated at different locations within a hydrothermal system [*Guilbert and Frank*, 1986]. The exact composition and occurrence of different mineral assemblages results from a complex interaction between temperature, pressure, pH, and rock composition [*Guilbert and Frank*, 1986]. However, hematite, and other minerals, are observed in terrestrial hydrothermal systems in veins and disseminated throughout an alteration zone.

Large-scale hydrothermal systems have been proposed for Mars to explain the formation of valley networks by mobilization of groundwater and aquifer recharge [*Gulick*, 1998]. Reassessment of these systems by *Harrison and Grimm* [1999] suggests that they may be less likely to generate the amount of near-surface water necessary to produce valley networks, but their occurrence on Mars remains a distinct possibility.

The primary argument against formation by precipitation from hot, Fe-rich fluids in hydrothermal zones is the large areal extent ($>10^5$ square km) of the region of exposed hematite. On Earth, veins of hematite are relatively small and occupy a small fraction of the total rock volume [*Guilbert and Frank*, 1986]. In addition, terrestrial hydrothermal systems typically have mineralized zones containing other minerals in addition to hematite. Finally, this region of Sinus Meridiani does not appear to be an obvious hydrothermal region because there is no evidence for major, near-surface volcanic activity to provide a heat source.

**4.5.3. Low-temperature dissolution and precipitation: Leaching.** On Earth, Fe-rich laterites and ferricretes form where Fe-rich humic acids or acid-sulfate waters are abundant and extensive gravity-driven leaching by surface water has oc-

curred [*Guilbert and Frank*, 1986]. The formation of Fe-rich laterites depends critically on the Eh and pH conditions. Mafic minerals and feldspars are unstable in acidic reducing waters and weather to form stable iron- and aluminum-rich oxides. These iron and aluminum oxide-hydroxides go into solution in a colloidal state and can be transported in low Eh and pH conditions [*Guilbert and Frank*, 1986]. They are redeposited where Eh and pH are high to form concretionary pisoliths [*Selby*, 1993]. On Earth, Fe-rich laterites form most readily in regions between the annual high and low water table positions and in regions of high rainfall with alternating wet and dry periods [*McFarlane*, 1976; *Selby*, 1993].

The primary argument against Fe-rich laterite formation is the requirement for extensive surface water to produce extensive leaching. In addition, these soils are generally red (because of the presence of red hematite) and thus do not meet our requirement for gray hematite. However, some process (e.g., burial metamorphism) may have converted the red hematite to gray hematite. This model is perhaps the most speculative of those presented here because it requires significant amounts of surface water, which would be expected to produce a far more extensive and diverse set of landforms than is observed.

**4.5.4. Surface weathering and coatings.** A variant of low-temperature precipitation is the formation of surface coatings by interaction of Fe-bearing rocks with surface and/or atmospheric water. Red hematite is a common product of weathering and alteration in the terrestrial environment [e.g., *Cornell and Schwertmann*, 1996]. However, if the hematite formed on the surface, then it is difficult to explain its occurrence only in the sm unit within Sinus Meridiani and the lack of hematite coatings or evidence for surface water processes elsewhere. Furthermore, red hematite is not consistent with TES and HST observations.

**4.5.5. Oxidation of magnetite-rich lava.** Another possible origin for Sinus Meridiani hematite is oxidation of coarse-grained lithogenic magnetite or low-Ti titanomagnetite. Localized Martian basalts could have been unusually rich in magnetite, which subsequently altered to hematite. To test this possibility, a $<1$ mm powder of naturally occurring magnetite (Ishpming, Michigan) was heated at 400°C in air for 4 hours. The emissivity spectra of the unheated and heated magnetite powders are shown in Figure 12. The magnetite fundamental vibration at $\sim$550 $cm^{-1}$ is clearly visible in the unheated sample. The spectrum of the heated sample is dominated by the two hematite fundamental vibrations at 450 and 525 $cm^{-1}$. Residual magnetite, presumably concentrated in the magnetite-rich cores of the particles, contributes the high emissivity in the region between 700 and 1400 $cm^{-1}$.

The primary argument against this model is the lack of distinct evidence for lava flows in the Sinus Meridiani sm unit on which the hematite occurs. In addition, as discussed above, the eroded morphology of sm and the fact that remnant craters remain intact when sm is removed suggest that this unit is more friable than primary lava. Unit sm could be a sedimentary deposit of oxidized magnetite-rich basalt transported into this region, but this model would require three separate processes (production of magnetite-rich lava, oxidation at elevated temperatures, and transport and sedimentation) to form the sm unit. This model does not necessarily require liquid water to accomplish oxidation, but water could be the agent to transport the gray hematite to Sinus Meridiani or expose it as a lag deposit.

### 4.6. Implications for Mars History

With one exception the models presented above all involve significant amounts of liquid water interacting at or near the surface. The presence of liquid water on Mars has been suggested by many authors (see recent reviews by *Carr* [1996] and *Baker et al*. [1992]). This water could have been stable in the ancient environment, indicating that Mars was "wetter and warmer" either early in its history [e.g., *Pollack et al*., 1987] or during more recent episodes [*Parker et al*., 1993; *Baker et al*., 1991; *Kargel and Strom*, 1992; *Gulick et al*., 1997], or they could have been out of equilibrium with the climate but sufficiently insulated by ice and dust to have existed for extended periods of time before sublimating or freezing [e.g., *McKay and Davis*, 1991]. The near-surface water either could have existed for short periods of time or could have occurred beneath the surface in ice-covered bodies of water or subsurface groundwater or hydrothermal systems.

*Calvin* [1998] has argued that visible/near-IR spectra of dark regions can be matched by spectral mixtures that include dark alteration minerals. These materials can occur in regions of outflow channels and basins, suggesting an origin by aqueous alteration [*Calvin*, 1998]. The occurrence of hematite in the low-albedo regions of Sinus Meridiani provides evidence that alteration can be associated with dark materials and that alteration is not restricted to bright regions on Mars.

One of the most significant aspects of the Sinus Meridiani hematite deposit is the lack of similar, large deposits exposed elsewhere in the equatorial region. The limited extent of this deposit places important constraints on its formation mechanism and the history of Mars. We know of no simple reason that any of the formation mechanisms suggested above would result in crystalline gray hematite formation being limited to only one place on Mars. Oxide iron formations should occur at various places where oxygenated, Fe-rich liquid water occurs. On Earth these deposits are widespread in both time and space. It is also unlikely that basalt flows that are particularly rich in lithogenic magnetite would occur at only one place. Similarly, hydrothermal processes are more likely around the large Martian volcanic constructs or large impact craters, and leaching by surface water (and other landforms associated with warm, wet conditions) would likely be widespread if water was stable near the surface.

Complete mapping of Mars by MGS TES will help to establish the extent to which other hematite-rich areas like the Sinus Meridiani occur. The number of areas, their geological context, and other remote-sensing data (e.g., HST spectral data) will provide important clues for understanding the origin of these hematite-rich regions.

### 4.7. Implications for Future Landing Sites

On the basis of the possible origin by precipitation from water, oxidation and/or precipitation by hydrothermal processes, or leaching by water, it appears that the crystalline gray hematite in Sinus Meridiani is indicative of some process or processes involving liquid water as well as the possibility of near-surface heat. This unique region therefore should be considered as a possible landing site for future Mars Surveyor missions that are searching for biotic and prebiotic environments. In addition, the relatively large size and smooth surface, equatorial position, moderate thermal inertia and rock abundance, and low elevation of the hematite-rich region satisfy engineering requirements for the near-term landed missions.

## 5. Conclusions

From the analysis of TES data returned during the aerobraking and science phasing portions of the MGS mission, we reach the following conclusions regarding the observations of a unique spectral component on Mars.

1. The TES data have identified a unique, localized, surface occurrence of hematite approximately 350 by 350–750 km in size in Sinus Meridiani.

2. TES spectra are well matched to crystalline red or gray hematite, rather than nanophase hematite, that has particle diameters $>10$ $\mu$m and possibly up to hundreds of micrometers. Exceptionally high (25–60%) abundances of fine-grained red hematite would be required to match the TES spectra, but these abundances are not observed in HST VNIR data. Therefore our preferred interpretation is that the Sinus Meridiani hematite is gray and not red.

3. The abundance of hematite required to match the TES spectra varies from $\sim$10% for particles $>30$ $\mu$m to 25–60% for $<10$ $\mu$m particles.

4. The Sinus Meridiani hematite-rich surface is associated with a smooth, layered, friable unit of probable sedimentary origin.

5. The processes that we considered for the formation of an extensive deposit of crystalline gray hematite fall into two classes depending on whether they require a significant amount of near-surface water: first, chemical precipitation that includes origin by (1) precipitation from oxygenated, Fe-rich water (oxide iron formations), (2) precipitation from Fe-rich hydrothermal fluids, (3) low-temperature dissolution and precipitation through mobile groundwater leaching, and (4) formation of surface coatings, and, second, thermal oxidation of magnetite-rich lavas. The formation of red hematite by weathering and alteration is not consistent with the coarse, gray crystalline hematite observed in Sinus Meridiani. None of these models can be eliminated on the basis of currently available data, but precipitation from Fe-rich water may be a slightly more plausible hypothesis based on the association with an apparent sedimentary unit, the extensive size, the distance from a near-surface regional heat source, and the lack of evidence for extensive surface water interactions elsewhere on Mars.

6. Because of the significance of water in the Sinus Meridiani region, it should be considered as a possible landing site for future Mars Surveyor missions that are searching for biotic and prebiotic environments. The physical characteristics of this site (extensive size, relatively smooth surface, equatorial position, moderate thermal inertia and rock abundance, and low elevation) satisfy the engineering requirements for the lander missions currently planned.

**Acknowledgments.** We wish to thank the entire TES Engineering Team, lead by Steve Silverman and Martin Greenfield at Raytheon Santa Barbara Remote Sensing, and Greg Mehall at Arizona State University for their efforts in developing the TES instrument. We thank Greg Mehall, Kelly Bender, Noel Gorelick, Kamran Qazi, Saadat Anwar, Michael Weiss-Malik, and Tara Haden for their excellent work in planning, acquiring, and processing the TES data at ASU. Finally, we wish to acknowledge our appreciation of the outstanding efforts of the MGS Spacecraft Teams at Lockheed Martin and NASA's Jet Propulsion Laboratory that have led to the success of the MGS mission. Excellent reviews by Wendy Calvin and Jeff Johnson significantly improved the manuscript. This work was supported by the Mars Global Surveyor Project Office and the NASA Planetary Geology and Geophysics Program. R. V. M. was supported by NASA's Cosmochemistry Program under RTOP 344-31-20-24. Contributed work was performed while M. D. L. held a National Research Council-JSC Research Associateship.

## References

Adams, J. B., M. O. Smith, and P. E. Johnson, Spectral mixture modeling: A new analysis of rock and soil types at the Viking Lander 1 site, *J. Geophys. Res*., *91*, 8098–8112, 1986.

Antoniadi, E. M., *La Planète Mars*, Hermann, Paris, 1930.

Baker, V. R., R. G. Strom, V. C. Gulick, J. S. Kargel, G. Komatsu, and V. S. Kale, Ancient oceans, ice sheets, and the hydrological cycle on Mars, *Nature*, *352*, 589–862, 1991.

Baker, V. R., M. H. Carr, V. C. Gulick, C. R. Williams, and M. S. Marley, Channels and valley networks, in *Mars*, edited by H. H. Kieffer et al., pp. 493–522, Univ. of Ariz. Press, Tucson, 1992.

Bandfield, J. L., P. R. Christensen, and M. D. Smith, Spectral data set factor analysis and end-member recovery: Application to analysis of Martian atmospheric particulates, *J. Geophys. Res*., this issue.

Banin, A., B. C. Clark, and H. Wanke, Surface chemistry and mineralogy, in *Mars*, edited by H. H. Kieffer et al., pp. 594–625, Univ. of Ariz. Press, Tucson, 1992.

Bell, J. F., III, Iron, sulfate, carbonate, and hydrated minerals on Mars, in *Mineral Spectroscopy: A Tribute to Roger G. Burns*, edited by M. D. Dyar, C. McCammon, and M. W. Schaefer, *Spec. Publ. Geochem. Soc*., *5*, 359–380, 1996.

Bell, J. F., III, and R. V. Morris, Identification of hematite on Mars from HST, *Lunar Planet. Sci*., *XXX*, 1999.

Bell, J. F., III, R. V. Morris, and J. B. Adams, Thermally altered palagonitic tephra: A spectral and process analog to the soils and dust of Mars, *J. Geophys. Res*., *98*, 3373–3385, 1993.

Bell, J. F., III, et al., Mineralogic and compositional properties of Martian soil and dust: Results from Mars Pathfinder, *J. Geophys. Res*., *105*, 1721–1755, 2000.

Bishop, J. L., and E. Murad, Schwertmannite on Mars? Spectroscopic analyses of schwertmannite, its relationship to other ferric minerals, and its possible presence in the surface material on Mars, in *Mineral Spectroscopy: A Tribute to Roger G. Burns*, edited by M. D. Dyar, C. McCammon, and M. W. Schaefer, *Spec. Publ. Geochem. Soc*., *5*, 337–358, 1996.

Burns, R. G., Rates and mechanisms of chemical weathering of ferromagnesian silicate minerals on Mars, *Geochim. Cosmochim. Acta*, *57*, 4555–4574, 1993.

Calvin, W. M., Could Mars be dark and altered?, *Geophys. Res. Lett*., *25*, 1597–1600, 1998.

Carr, M. H., *Water on Mars*, Oxford Univ. Press, New York, 1996.

Christensen, P. R., The spatial distribution of rocks on Mars, *Icarus*, *68*, 217–238, 1986.

Christensen, P. R., Variations in Martian surface composition and cloud occurrence determined from thermal infrared spectroscopy: Analysis of Viking and Mariner 9 data, *J. Geophys. Res*., *103*, 1733–1746, 1998.

Christensen, P. R., Calibration report for the Thermal Emission Spectrometer (TES) for the Mars Global Surveyor Mission, Mars Global Surveyor Project, Jet Propul. Lab., Pasadena, Calif., 1999.

Christensen, P. R., and H. J. Moore, The Martian surface layer, in *Mars*, edited by H. H. Kieffer et al., pp. 686–729, Univ. of Ariz. Press, Tucson, 1992.

Christensen, P. R., et al., Thermal Emission Spectrometer experiment: The Mars Observer Mission, *J. Geophys. Res*., *97*, 7719–7734, 1992.

Christensen, P. R., et al., Results from the Mars Global Surveyor Thermal Emission Spectrometer investigation, *Science*, *279*, 1692–1698, 1998.

Christensen, P. R., J. L. Bandfield, M. D. Smith, V. E. Hamilton, and R. N. Clark, Identification of a basaltic component on the Martian surface from Thermal Emission Spectrometer data, *J. Geophys. Res*., this issue.

Clark, B. C., A. K. Baird, R. J. Weldon, D. M. Tsusaki, L. Schnabel, and M. P. Candelaria, Chemical composition of Martian fines, *J. Geophys. Res*., *87*, 10,059–10,067, 1982.

Clark, R. N., and P. G. Lucey, Spectral properties of ice-particulate mixtures and implications for remote sensing, 1, Intimate mixtures, *J. Geophys. Res*., *89*, 6341–6348, 1984.

Clark, R. N., A. J. Gallagher, and G. A. Swayze, Material absorption band depth mapping of imaging spectrometer data using a complete band shape least-squares fitting with library reference spectra, in

*Proceedings of the Second Airborne Visible/Infrared Imaging Spectrometer (AVIRIS) Workshop*, *Jet. Propul. Lab. Publ. 90-54*, 176–186, 1990.

Cornell, R., and U. Schwertmann, *The Iron Oxides: Structure, Properties, Reactions, Occurrences, and Uses*, 573 pp., VCH, New York, 1996.

Curi, N., and D. P. Franzmeier, Effect of parent rocks on chemical and mineralogical properties of some oxisols in Brazil, *Soil Sci. Soc. Am. J.*, *51*, 153–158, 1987.

Edgett, K. S., Nature and source of low-albedo surface material in the sandy aeolian environment of Sinus Meridiani, Mars, *Geol. Soc. Am. Abstr. Programs*, *29*, A214, 1997.

Edgett, K. S., Mars surface properties: Dark mantles of regional and local extent, *Abstracts with Geol. Soc. Am. Abstr. Programs*, *31*, 1999.

Edgett, K. S., and T. J. Parker, Water on early Mars: Possible subaqueous sedimentary deposits covering ancient cratered terrain in western Arabia and Sinus Meridiani, *Geophys. Res. Lett.*, *24*, 2897–2900, 1997.

Evans, D. L., and J. B. Adams, Comparison of Viking Lander multispectral images and laboratory reflectance spectra of terrestrial samples, *Proc. Lunar Planet. Sci. Conf.*, *10th*, 1829–1834, 1979.

Farmer, V. C., *The Infrared Spectra of Minerals*, edited by V. C. Farmer, pp. 227–331, Adlard and Son Ltd., 1974.

Frutos, J., and J. Oyarzun, Tectonic and geochemical evidence concerning the genesis of El Laco lava flow deposits, Chile, *Econ. Geol.*, *70*, 988–990, 1975.

Golombek, M. P., H. J. Moore, A. F. C. Haldemann, T. J. Parker, and J. T. Schofield, Assessment of Mars Pathfinder landing site predictions, *J. Geophys. Res.*, *104*, 8585–8594, 1999.

Greeley, R., and J. E. Guest, Geologic map of the eastern equatorial region of Mars, *U.S. Geol. Surv. Misc. Invest. Map*, *I-1802-B*, 1987.

Guilbert, J. M., and C. F. Frank Jr., *The Geology of Ore Deposits*, W. H. Freeman, New York, 1986.

Gulick, V. C., Magmatic intrusions and a hydrothermal origin for fluvial valleys on Mars, *J. Geophys. Res.*, *103*, 19,365–19,388, 1998.

Gulick, V. C., D. Tyler, C. P. McKay, and R. M. Haberle, Episodic ocean-induced $CO_2$ greenhouse on Mars: Implications for fluvial valley formation, *Icarus*, *130*, 68–86, 1997.

Hancock, K. R., Mineral pigments, in *Industrial Minerals and Rocks*, edited by S. J. Lefond, pp. 335–357, Am. Inst. of Min., Metal., and Pet. Eng., Inc., New York, 1975.

Hapke, B., Combined theory of reflectance and emittance spectroscopy, in *Remote Geochemical Analysis: Elemental and Mineralogical Composition*, edited by C. M. Pieters and P. A. J. Englert, Cambridge Univ. Press, New York, 1993.

Harrison, K. P., and R. E. Grimm, A conservative approach to hydrothermal systems on Mars, *Lunar Planet. Science*, *XXX*, abstract 1941, 1999.

Hunt, G. R., and L. M. Logan, Variation of single particle mid-infrared emission spectrum with particle size, *Appl. Opt.*, *11*, 142–147, 1972.

Hunt, G. R., L. M. Logan, and J. W. Salisbury, Mars: Components of infrared spectra and the composition of the dust cloud, *Icarus*, *18*, 459–469, 1973.

Kargel, J. S., and R. G. Strom, Ancient glaciation on Mars, *J. Geol.*, *20*, 3–7, 1992.

Kirkland, L. E., K. C. Kerr, and P. B. Forney, Comparison of 1969 IRS and IRIS spectra to TES, paper presented at Fifth International Mars Science Conference, Calif. Inst. of Technol., Pasadena, Calif., 1999.

Lane, M. D., Midinfrared optical constants of calcite and their relationship to particle size effects in thermal emission spectra of granular calcite, *J. Geophys. Res.*, *104*, 14,099–14,108, 1999.

McFarlane, M. J., *Laterite and Landscape*, Academic, San Diego, Calif., 1976.

McKay, C. P., and W. L. Davis, Duration of liquid water habitats on early Mars, *Icarus*, *90*, 214–221, 1991.

McSween, H. Y., Jr., et al., Chemical, multispectral, and textural constraints on the composition and origin of rocks at the Mars Pathfinder landing site, *J. Geophys. Res.*, *104*, 8679–8716, 1999.

Merenyi, E., R. B. Singer, and J. S. Miller, Mapping of spectral variations on the surface of Mars from high spectral resolution telescopic images, *Icarus*, *124*, 280–295, 1996.

Moersch, J. E., and P. R. Christensen, Thermal emission from particulate surfaces: A comparison of scattering models with measured spectra, *J. Geophys. Res.*, *100*, 7465–7477, 1995.

Moore, H. J., R. E. Hutton, R. F. Scott, C. R. Spitzer, and R. W. Shorthill, Surface materials of the Viking landing sites, *J. Geophys. Res.*, *82*, 4497–4523, 1977.

Moore, H. J., C. R. Spitzer, K. Z. Bradford, P. M. Cates, E. Hutton, and R. W. Shorthill, Sample fields of the Viking Landers: Physical properties and aeolian processes, *J. Geophys. Res.*, *84*, 8365–8377, 1979.

Moore, H. J., C. D. Clow, and R. E. Hutton, A summary of Viking sample-trench analysis for angles of internal friction and cohesions, *J. Geophys. Res.*, *87*, 10,043–10,050, 1982.

Morris, R. C., Genetic modeling for banded iron formation of the Hamersley Group, Pilbara Craton, Western Australia, *Precambrian Res.*, *60*, 243–246, 1993.

Morris, R. V., and D. C. Golden, Goldenrod pigments and the occurrence of hematite and possibly goethite in the Olympus-Amazonis region of Mars, *Icarus*, *134*, 1–10, 1998.

Morris, R. V., H. V. Lauer, C. A. Lawson, E. K. Gibson, G. A. Nace, and C. Stewart, Spectral and other physiochemical properties of submicron powders of hematite ($\alpha$-$Fe_2O_3$), maghemite ($\gamma$-$Fe_2O_3$), magnetite ($Fe_3O_4$), goethite ($\alpha$-FeOOH), and leipocrocite ($\gamma$-FeOOH), *J. Geophys. Res.*, *90*, 3126–3144, 1985.

Morris, R. V., D. G. Agresti, H. V. Lauer, J. A. Newcomb, T. D. Shelfer, and A. V. Murali, Evidence for pigmentary hematite on Mars based on optical, magnetic, and Mossbauer studies of super paramagnetic (nanocrystalline) hematite, *J. Geophys. Res.*, *94*, 2760–2778, 1989.

Morris, R. V., J. H. V. Lauer, D. G. Schulze, and R. G. Burns, *Proc. Lunar Planet. Sci. Conf.*, *22nd*, 927, 1991.

Morris, R. V., D. C. Golden, J. F. Bell III, H. V. J. Lauer, and J. B. Adams, Pigmenting agents in Martian soils: Inferences from spectral, Mössbauer, and magnetic properties of nanophase and other iron oxides in Hawaiian palagonitic soil PN-9, *Geochim. Cosmochim. Acta*, *57*, 4597–4609, 1993.

Morris, R. V., D. W. Ming, D. C. Golden, and J. F. Bell III, An occurrence of jarositic tephra on Mauna Kea, Hawaii: Implications for the ferric mineralogy of the Martian surface, in *Mineral Spectroscopy: A Tribute to Roger G. Burns*, edited by M. D. Dyar, C. McCammon, and M. W. Schaefer, *Spec. Publ. Geochem. Soc.*, *5*, 327–336, 1996.

Morris, R. V., D. C. Golden, and J. F. Bell III, Low-temperature reflectivity spectra of red hematite and the color of Mars, *J. Geophys. Res.*, *102*, 9125–9133, 1997.

Morris, R. V., et al., Mineralogy, composition, and alteration of Mars Pathfinder rocks and soils: Evidence from multispectral elemental, and magnetic data on terrestrial analogue, SNC meteorite, and Pathfinder samples, *J. Geophys. Res.*, *105*, 1757–1817, 2000.

Murchie, S., J. Mustard, J. Bishop, J. Head, C. Pieters, and S. Erard, Spatial variations in the spectral properties of bright regions on Mars, *Icarus*, *105*, 454–468, 1993.

Mustard, J. F., and J. F. Bell III, New composite reflectance spectra of Mars from 0.4 to 3.14 $\mu$m, *Geophys. Res. Lett.*, *21*, 353–356, 1994.

Palluconi, F. D., and H. H. Kieffer, Thermal inertia mapping of Mars from 60°S to 60°N, *Icarus*, *45*, 415–426, 1981.

Park, C. F., Jr., A magnetite "flow" in northern Chile, *Econ. Geol.*, *56*, 431–441, 1961.

Parker, T. J., D. S. Gorsline, R. S. Saunders, D. C. Pieri, and D. M. Schneeberger, Coastal geomorphology of the Martian northern plains, *J. Geophys. Res.*, *98*, 11,061–11,078, 1993.

Pollack, J. B., J. F. Kasting, S. M. Richardson, and K. Poliakoff, The case for a wet, warm climate on early Mars, *Icarus*, *71*, 203–224, 1987.

Powell, C. M., N. H. S. Oliver, D. M. M. Z.-X. Li, and J. Ronaszeki, Synorogenic hydrothermal origin for giant Hamersley iron oxide ore bodies, *Geology*, *27*, 175–178, 1999.

Presley, M. A., The origin and history of surficial deposits in the central equatorial region of Mars, M.A. thesis, Washington Univ., St. Louis, Mo., 1986.

Presley, M. A., and P. R. Christensen, Thermal conductivity measurements of particulate materials, 2, Results, *J. Geophys. Res.*, *102*, 6651–6566, 1997.

Ramanaidou, E., D. Nahon, A. Decarreau, and A. J. Melfi, Hematite and goethite duracrusts developed by lateritic chemical weathering of Precambrian banded iron formations, Minas Gerais, Brazil, *Clay Miner.*, *44*, 22–31, 1996.

Reider, R., T. Economou, H. Wanke, A. Turkevich, J. Crisp, J. Bruckner, G. Drebus, and H. Y. McSween Jr., The chemical composition of Martian soil and rocks returned by the mobile alpha proton X-ray

spectrometer: Preliminary results from the X-ray mode, *Science*, *278*, 1771–1774, 1997.

Rendon, J. L., and C. J. Serna, IR spectra of powder hematite: Effects of particle size and shape, *Clay Miner*., *16*, 375–381, 1981.

Roush, T. L., D. L. Blaney, and R. B. Singer, The surface composition of Mars as inferred from spectroscopic observations, in *Remote Geochemical Analysis: Elemental and Mineralogical Composition*, edited by C. M. Pieters and P. A. J. Englert, Cambridge Univ. Press, New York, 1993.

Ruff, S. W., P. R. Christensen, P. W. Barbera, and D. L. Anderson, Quantitative thermal emission spectroscopy of minerals: A technique for measurement and calibration, *J. Geophys. Res*., *102*, 14,899–14,913, 1997.

Salisbury, J. W., and J. W. Eastes, The effect of particle size and porosity on spectral contrast in the mid-infrared, *Icarus*, *64*, 586–588, 1985.

Salisbury, J. W., L. S. Walter, N. Vergo, and D. M. D'Aria, *Infrared (2.1–25 μm) Spectra of Minerals*, 267 pp., Johns Hopkins Univ. Press, Baltimore, Md., 1991.

Schaefer, M. W., Are there abiotically-precipitated iron-formations on Mars?, in *Mineral Spectroscopy: A Tribute to Roger G. Burns*, edited by M. D. Dyar, C. McCammon, and M. W. Schaefer, *Spec. Publ. Geochem. Soc*., *5*, 381–393, 1996.

Schultz, P. H., and A. B. Lutz, Polar wandering on Mars, *Icarus*, *73*, 91–141, 1988.

Scott, D., and K. Tanaka, Geologic map of the Western Equatorial Region of Mars, scale 1:15,000,000, *U.S. Geol. Surv. Misc. Invest. Ser. Map I-1802-A*, 1986.

Selby, M. B., *Hillslope Materials and Processes*, Oxford Univ. Press, New York, 1993.

Serna, C. J., J. L. Rendon, and J. E. Iglesias, Infrared surface modes in the corundum-type microcrystalline oxides, *Spectrochim. Acta*, *Part A*, *38*, 797–802, 1982.

Singer, R. B., Spectral evidence for the mineralogy of high-albedo soils and dust on Mars, *J. Geophys. Res*., *87*, 10,159–10,168, 1982.

Smith, M. D., J. Pearl, B. Conrath, and P. R. Christensen, Mars Global Surveyor Thermal Emission Spectrometer (TES) observations of dust opacity during aerobraking and science phasing, *J. Geophys. Res*., this issue (a).

Smith, M. D., J. L. Bandfield, and P. R. Christensen, Separation of atmospheric and surface spectral features in Mars Global Surveyor Thermal Emission Spectrometer (TES) spectra, *J. Geophys. Res*., this issue (b).

Soderblom, L. A., The composition and mineralogy of the Martian surface from spectroscopic observations: 0.3 μm to 50 μm, in *Mars*, edited by H. H. Kieffer et al., pp. 557–593, Univ. Ariz. Press, Tucson, 1992.

Toulmin, P., III, A. K. Baird, B. C. Clark, K. Keil, J. H. J. Rose, R. P. Christian, P. H. Evans, and W. C. Kelliher, Geochemical and mineralogical interpretation of the Viking inorganic chemical results, *J. Geophys. Res*., *82*, 4625–4634, 1977.

U.S. Geological Survey, Topographic map of Mars, scale 1:25,000,000, *U.S. Geol. Surv. Misc. Invest. Map*, *I-2179*, 1991.

Vincent, R. K., and G. R. Hunt, Infrared reflectance from mat surfaces, *Appl. Opt*., *7*, 53–59, 1968.

J. L. Bandfield, P. R. Christensen, V. E. Hamilton, and S. W. Ruff, Department of Geology, Arizona State University, Tempe AZ 85287. (phil@elex.la.asu.edu)

R. N. Clark, T. Hoefen, and R. Pearson, U.S. Geological Survey, Denver, CO 80225.

K. S. Edgett and M. C. Malin, Malin Space Science Systems, San Diego, CA 92191.

H. H. Kieffer, U.S. Geological Survey, Flagstaff, AZ 86001.

R. O. Kuzmin, Vernadsky Institute, Moscow, Russia.

M. D. Lane and R. V. Morris, Johnston Space Center, Houston, TX 77058.

J. C. Pearl and M. D. Smith, Goddard Space Flight Center, Greenbelt, MD 20771.

T. L. Roush, Ames Research Center, Moffett Field, CA 94035.

(Received May 25, 1999; revised October 5, 1999;
accepted October 12, 1999.)